JOURNAL OF CHEMICAL INFORMATION AND MODELING

Article

pubs.acs.org/jcim

Revised Basin-Hopping Monte Carlo Algorithm for Structure Optimization of Clusters and Nanoparticles

Gustavo G. Rondina*,† and Juarez L. F. Da Silva*,‡

†Instituto de Física de São Carlos, Universidade de São Paulo, Caixa Postal 369, 13560-970, São Carlos, SP, Brazil

‡Instituto de Química de São Carlos, Universidade de São Paulo, Caixa Postal 780, 13560-970, São Carlos, SP, Brazil

Supporting Information

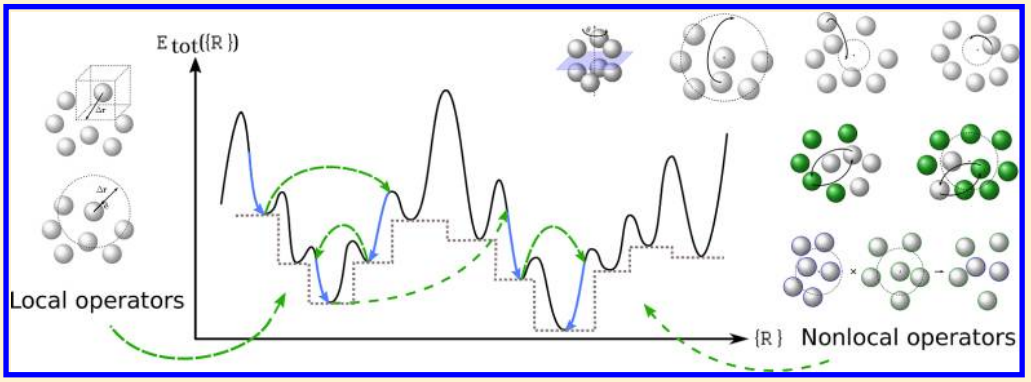

ABSTRACT: Suggestions for improving the Basin-Hopping Monte Carlo (BHMC) algorithm for unbiased global optimization of clusters and nanoparticles are presented. The traditional basin-hopping exploration scheme with Monte Carlo sampling is improved by bringing together novel strategies and techniques employed in different global optimization methods, however, with the care of keeping the underlying algorithm of BHMC unchanged. The improvements include a total of eleven local and nonlocal trial operators tailored for clusters and nanoparticles that allow an efficient exploration of the potential energy surface, two different strategies (static and dynamic) of operator selection, and a filter operator to handle unphysical solutions. In order to assess the efficiency of our strategies, we applied our implementation to several classes of systems, including Lennard-Jones and Sutton-Chen clusters with up to 147 and 148 atoms, respectively, a set of Lennard-Jones nanoparticles with sizes ranging from 200 to 1500 atoms, binary Lennard-Jones clusters with up to 100 atoms, $(AgPd)_{55}$ alloy clusters described by the Sutton-Chen potential, and aluminum clusters with up to 30 atoms described within the density functional theory framework. Using unbiased global search our implementation was able to reproduce successfully the great majority of all published results for the systems considered and in many cases with more efficiency than the standard BHMC. We were also able to locate previously unknown global minimum structures for some of the systems considered. This revised BHMC method is a valuable tool for aiding theoretical investigations leading to a better understanding of atomic structures of clusters and nanoparticles.

I. INTRODUCTION

Metallic clusters (few to few hundreds atoms) and nanoparticles (few hundreds to few thousands atoms) have been the focus of a large number of experimental and theoretical studies and have put forth a science of their own, spanning across a diversity of fields, such as physics, chemistry, biology, and engineering.[1] This interest arises from the fact that those particles have physical and chemical properties that differ from both their individual constituents and their bulk counterparts,[2] including optical,[3] magnetic,[4] electronic,[5] and reactivity[6] properties. These properties are highly dependent on their particular characteristics, such as size, shape, and composition, mainly due to quantum size effects. Several studies have suggested that it is possible to control these characteristics in order to tune the physical and chemical properties, opening the possibility for a wide range of technological applications which may bring a wealth of benefits to the society.

For instance, ethanol production from syngas is enhanced by placing rhodium (Rh) clusters inside carbon nanotubes.[7] Gold (Au) nanoparticles (NPs) conjugated with specific antibodies can be used as biosensors in surface plasmon resonance imaging to help distinguish cancerous from noncancerous cells.[8] Narayanan and El-Sayed[9] reported that the shape of platinum (Pt) NPs plays an important role in their catalytic activity, with the activation energy of particular reactions varying among tetrahedral, cubical, and spherical structures. Scholl et al.[10] investigated the plasmon resonance of silver (Ag) NPs with sizes from 2 to 20 nm and found deviations from classical to quantum regime with decreasing size, specially below 10 nm. All those studies indicate clearly that the atomic structure and shape play an important role in the physical and

Received: April 12, 2013
Published: August 20, 2013

   dx.doi.org/10.1021/ci400224z | J. Chem. Inf. Model. 2013, 53, 2282−2298

chemical behavior of clusters and NPs, and hence, a complete knowledge of the atomic structure of these particles is a prerequisite to understand and exploit their properties for technological applications.

The task of determining the structure of a particle which minimizes its total energy is a global optimization problem that consists in finding the global minimum of the potential energy surface (PES). As the number of atoms increases, the complexity of the problem grows, and, for instance, for Lennard-Jones (LJ) particles, it has been suggested[11,12] that the number of local minima increases exponentially with system size. Wales and Doye[13,14] have confirmed this behavior, also showing it holds true for the number of transition states of the PES. This poses a great challenge for global optimization algorithms, given that sampling all existing minima is unpractical except for very small sizes. It has been known that features in the PES favor the discovery of the global minima, as it is the case of a PES containing a single funnel-like topology, or a single principal minimum surrounded by weak noise. In other cases, multiple funnels regions are separated by high energy barriers, and competing low-lying configurations offer a much more difficult scenario for global optimization.[15]

Several global optimization algorithms have been developed to obtain the global minimum of clusters and NPs, such as genetic algorithms[16−19] (GA) based on evolutionary techniques, basin-hopping (BH) methods such as the Basin-Hopping Monte Carlo[15,20,21] (BHMC), which combines Monte Carlo (MC) and local optimization algorithms, conformational space annealing,[22] dynamic lattice search,[23] population based methods,[24] probabilistic global search,[25] two-phase search methods,[26] etc. A detailed discussion on global optimization algorithms for particles can be found in refs 27−31.

The BHMC algorithm was first introduced by Li and Scheraga[32] under the name Monte Carlo with Minimization (MCM) as an approach to the multiple minima problem in protein folding. Wales and Doye generalized this method and applied it to several systems, including LJ clusters with sizes from 2 to 110 atoms[20] and Sutton-Chen (SC) clusters from 3 up to 80 atoms.[33] In the BHMC method, the PES is transformed by mapping each of its points onto the local minimum nearest to a particular point by employing a local minimization procedure. In contrast with most PES transformation methods, in the case of BHMC the relative positions and depths of the local minima, and thus of the global minimum, are not altered by the transformation, and therefore it is not necessary to employ a procedure to map the transformed PES back onto the original one, which is usually a difficult task. One of the consequences of this transformation in BHMC is that it allows the possibility to employ large atomic displacements when exploring the PES, in comparison with standard MC, for example, and hence it increases the rate at which the surface is explored.

Within the framework of BH algorithms many strategies have been suggested to improve their efficiency.[34−44] Leary[34] introduced the monotonic sequence BH, in which only downhill moves descending to the bottom of the PES funnels are allowed, with a restart technique to escape from these funnels, and with this method the author was able to find a previously unknown global minimum for the LJ_{98} cluster. Wales and Head-Gordon[45] improved the optimization of small proteins described by coarse-grained potentials by using BHMC with a similar restart procedure, as implemented in the public domain package GMIN.[46] Strodel et al.[47] successfully identified the most stable structures of peptide monomers and small oligomers using a global optimization scheme combining BH with parallel tempering, which is also available in GMIN.[46]

Locatelli and Schoen[35] proposed a transformation on the PES that reduces the number of stationary points and coupled it with a two-phase search using a monotonic BH algorithm, increasing the success rates for difficult LJ clusters. Zhan et al.[38] combined the BHMC and the multicanonical MC methods and showed that this approach is more effective for LJ clusters containing more than 150 atoms. Iwamatsu and Okabe[37] introduced a simple jump procedure that helps escaping deep local minima and moving to different regions of PES, which proved effective for difficult LJ cases. More recently, an approach exploring symmetry during the search for the global minimum has been employed with BHMC and GA, which increases the chances of finding the global minimum for LJ clusters.[48]

Most of those suggestions to extend BHMC beyond Wales and Doye[20] aimed at improving the success rate of the algorithm for empirical interacting potentials or at identifying new global minima configurations within these potentials. Only few attempts have been reported concerning methodologies combining BHMC with first-principles descriptions based on density functional theory (DFT),[21,49−53] which is a basic requirement to obtain an accurate assessment of the atomic structure of a given system, as first or second generation empirical potentials have great difficulties to provide a correct description of clusters and NPs with diameters of few nanometers. Furthermore, it is important to mention that the strategy of using BHMC with empirical potentials to determine candidate global minimum structures to be further refined by first-principles calculations might provide good results for particular cases;[54−61] however, this is not a general approach as the initial configurations are biased by the particular empirical potential. This combined strategy has been employed with other optimization methods as well, and early examples using GA include optimization of pure Au clusters[62] and binary AgNi and AgCu clusters.[63]

Although several strategies have been employed to take advantage of the BHMC algorithm in obtaining the global minima of clusters and NPs of technological interest, a general approach for treating particles described within the DFT framework requires an increase in efficiency of the method in order to decrease the total number of BHMC steps performed during the optimization, since DFT calculations have higher computational cost. Therefore, it is of great interest to have a methodology able to treat different classes of materials, comprising trial operators that can perform efficiently within unbiased methods, a desired feature in a general global optimization algorithm.

In this work, we revisit the BHMC algorithm by bringing together in a single framework ideas that have proven effective in different global optimization algorithms and also novel techniques to deal with the use of a large number of trial operators within BHMC. The resulting methodology is robust and general, with improved efficiency with respect to standard BHMC implementations in many cases, however, still maintaining the simplicity of the traditional BHMC algorithm, which is one of its hallmarks. The methodological strategies presented in this paper can be included in exiting BHMC implementations without major difficulties and can be used with empirical potentials and first-principles descriptions based on DFT. To test our suggestions, we applied our own

implementation to the global optimization of a wide range of particles, namely, LJ_N clusters (N = 2−147), larger LJ_N NPs (N = 200, 250, 300, ···, 1000, 1500), SC_N clusters (N = 3−148), binary LJ_N (BLJ_N) clusters (N = 5−100), binary transition-metal clusters, $(AgPd)_{55}$ described by the SC potential,[64,65] and Al_N clusters (N = 2−30) described within DFT.

II. METHODOLOGY

A. Standard Basin-Hopping Monte Carlo Algorithm. Finding the ground state configuration of a particle of N atoms consists in minimizing the PES with respect to the atomic positions, $\{\mathbf{R}\} = \mathbf{r}_1, \mathbf{r}_2, ..., \mathbf{r}_N$, in which the number of local minima increases exponentially with the number of atoms.[12−14] In the BHMC algorithm, the original PES, represented by $E_{tot}(\{\mathbf{R}\})$, is transformed by using a local optimization algorithm, e.g., Broyden-Fletcher-Goldfarb-Shanno (BFGS), steepest descent, conjugate gradient, etc.,[66] into a less intricate PES by the means of mapping each point in the configuration space onto a local minimum. This transformation can be expressed as $\tilde{E}_{tot}(\{\mathbf{R}\}) = min(E_{tot}(\{\mathbf{R}\}))$, defining basins of attraction,[32,20] Figure 1, and exploring it consists of a Monte Carlo sampling of the basins through random atomic displacements and the Metropolis criterion.

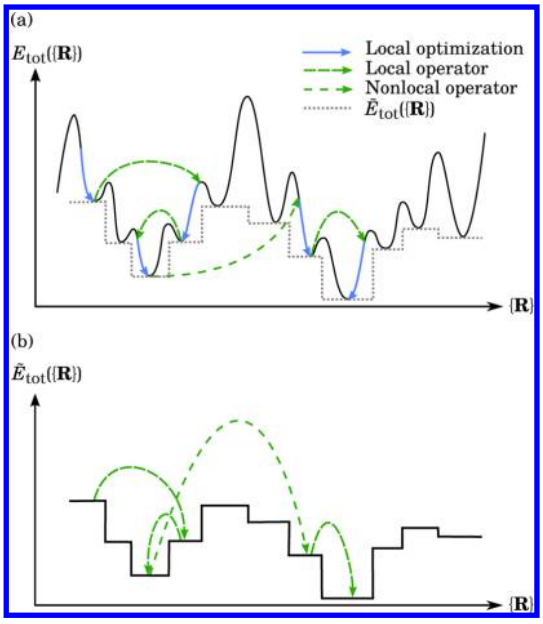

Figure 1. Simplified plot of a PES illustrating the main features of the BHMC algorithm. (a) Exploration of the PES is performed by using local optimization (solid blue lines) together with local and nonlocal trial operators (dashed green lines). The local optimization transforms the PES into one defined by a set of basins of attraction (dotted gray line). (b) Visualization of the BHMC algorithm acting on the transformed PES.

The main difference between the standard MC technique and the BHMC algorithm is the application of a local optimizer to each point of the PES. Since the exploration is performed by hopping among different basins, larger random atomic displacements, $\Delta\mathbf{r}_i$, are allowed in BHMC in comparison to standard MC. This feature contributes to increase the exploration of the PES and, hence, the success rate in obtaining the global minimum. Most BHMC implementations employ mainly simple atomic displacements to generate new configurations,[21,67,68] which is in contrast with different global optimization algorithms, such as the GA,[16,19] which employ several trial operators. With this in mind and aiming at improving the success rate of BHMC, in particular, employing unbiased randomly initialized atomic configurations, we propose a set of new strategies.

B. Revised Basin Hopping Monte Carlo Algorithm. Below we describe our BHMC implementation, containing suggestions and new strategies to employ a large set of trial operators, however, still using the Metropolis criterion with a single temperature, as in the standard BHMC algorithm.

1. Random Initialization. The initial particle configuration, $\{\mathbf{R}\}$, is randomly created within a spherical container or a cubic box of equal volumes. The sphere radius is calculated using the equation[69]

$$R = 2R_c\left[\frac{1}{2} + \left(\frac{3N}{4\pi\sqrt{2}}\right)^{1/3}\right] \quad (1)$$

where R_c is the average covalent radius of the M chemical species, defined as $R_c = (1/M)\Sigma_\alpha R_c^\alpha$. R_c^α is the covalent radius of the species α as reported in ref 70. For particles described by LJ and SC potentials with reduced units, R_c is taken as the average of half of the nearest neighbor distance. The cube root term in eq 1 is required to obtain the correct scaling of the volume as a function of the number of atoms.

To eliminate unphysical overlapping or disconnected atoms in the initial configuration, which can be specially important for BHMC-DFT calculations, the initial atomic positions are randomly generated within the container with the condition that the distance of atom i to its nearest neighbor j, d_{ij}, should satisfy the constraint $(1 - \gamma)R_c^{\alpha\beta} < d_{ij} < (1 + \gamma)R_c^{\alpha\beta}$, where γ is an adjustable parameter and $R_c^{\alpha\beta} = R_c^\alpha + R_c^\beta$. From our BHMC-DFT calculations, we found that γ = 0.20−0.40 yields good initial configurations as it minimizes problems in the electron density self-consistency. This condition is not strictly required for LJ and SC potentials as the total energy and forces are calculated using analytic equations, and most local optimization procedures can be adjusted to deal with situations of large gradients on the PES.

2. Local Optimization. In principle the local optimization procedure carried out in the BHMC algorithm can be of any nature, provided it guarantees that when applied to any input structure it will result in a local minimum of the PES. In this work, for LJ and SC clusters up to 147 and 148 atoms, respectively, the adaptive steepest descent algorithm was used, described in detail in the Appendix. For LJ nanoparticles ($N \geq$ 200) we used the Dai-Liao variant of the conjugate gradient algorithm.[71] For DFT calculations, the minimization employed was the BFGS algorithm with trusted region,[72] as implemented in the electronic structure package FHI-aims.[73]

3. Trial Operators. One of the key aspects determining the performance of the BHMC algorithm is how the trial configurations are generated, which are responsible for driving the search from one basin to another. In this study we propose the combination of a large set of trial operators, Figure 2, beyond simple random atomic displacements.[21,67,68] In our implementation we identify the trial operators as local and nonlocal, as shown in Figure 1, which work together to increase the mobility of the search over the PES. Nonlocal operators allow different regions to be reached, while local operators thoroughly explore each region. To our best knowledge, this is the first study to combine a set of 11 operators of different nature within the BHMC algorithm, maintaining the

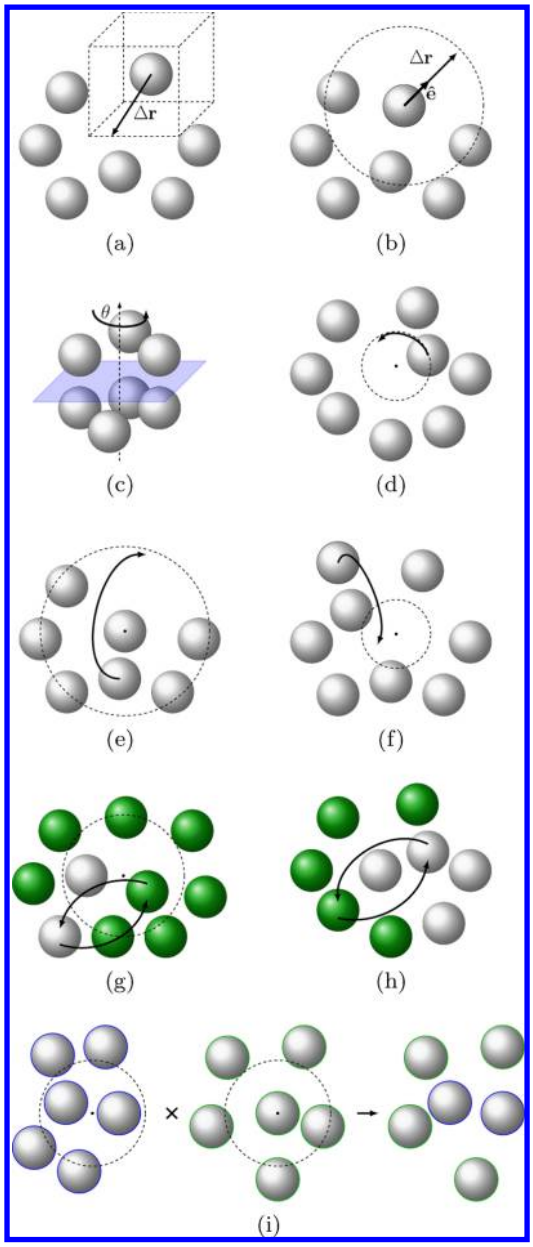

Figure 2. Some of the trial operators available in our BHMC implementation. (a) Cartesian displacement operator. (b) Geometric center displacement operator. (c) Twist operator. (d) Angular operator. (e) Surface angular operator. (f) Interior operator. (g) Exchange operator. (h) Geometric exchange operator. (i) Crossover operator. Wherever appropriate, the approximate geometric center of a cluster is indicated with a black dot.

Metropolis criterion unaltered and employing empirical or first-principles interacting potentials. In what follows we summarize the operators and provide pointers to help take advantage of each operator, and then we present strategies to combine all of them in a single run.

a. Atomic Displacement Operators – Local. These operators act on a set of atomic coordinates, $\mathbf{r}_i$, and randomly displace them around their original positions, which can be represented by

$$\mathbf{r}_i' = \mathbf{r}_i + \Delta\mathbf{r}_i \tag{2}$$

where $\mathbf{r}_i$ and $\mathbf{r}_i'$ are the old and new atomic positions of atom i, respectively, while $\Delta\mathbf{r}_i$ determines the magnitude, direction, and the dependence of the atomic displacements with the environment. In this study, we selected two approaches for calculating the displacements. The first is a modified version of the *cartesian displacement operator* (CDO) used in MC[74] and BHMC implementations[20,21]

$$\Delta\mathbf{r}_i = Sd_{ij}([-1, +1]_x\mathbf{x} + [-1, +1]_y\mathbf{y} + [-1, +1]_z\mathbf{z}) \tag{3}$$

where S is a constant parameter, and d_{ij} is calculated on the fly at every application of the operator. The parameter d_{ij} is a scaling factor that takes into account differences in the magnitude of the bond lengths, which is important for atoms near the surface and for particles composed by more than one chemical species. The notation $[-1, +1]$ indicates a random number drawn from a uniform distribution between −1 and +1, which is different for each displacement component, x, y, and z. The magnitude of the atomic displacements is always between 0 and Sd_{ij}, i.e., only one parameter, S, must be provided.

In the second approach, we employed a less common operator, named *geometric center displacement operator* (GCDO) in this work, that takes into account structural features of the particle, namely the distance of the atom i to the geometric center of the particle, by using the following equation[68]

$$\Delta\mathbf{r}_i = \left[(\alpha_{\max} - \alpha_{\min})\left(\frac{R_i}{R_{\max}}\right)^w + \alpha_{\min}\right] d_{ij}\hat{\mathbf{e}}_i(\theta_i, \phi_i) \tag{4}$$

where the parameters $\alpha_{\min}$ and $\alpha_{\max}$ provide lower and upper factors, respectively, to the magnitude of the displacement. R_i is the distance of atom i to the geometric center of the particle, and $R_{\max}$ corresponds to the particle radius, defined as the largest distance of an atom to the particle geometric center. Thus, $(R_i/R_{\max})^w$ introduces a dependence of the atomic displacement on the position of atom i relative to the geometric center with weight w. This operator is based on the physical expectation that atoms on the surface of a particle can execute larger displacements compared with inner core atoms. The random unit vector, $\hat{\mathbf{e}}_i(\theta_i, \phi_i)$, gives the radial direction of displacement. In contrast with eq 3, we must provide three parameters in eq 4 ($\alpha_{\min}$, $\alpha_{\max}$, w), which was modified from the original version in ref 68 to allow a better control of the atomic displacements at the center of the particle.

The amount of atoms affected by the CDO and GCDO is a parameter that can assume values from 1 up to N. Once this number is defined, the atoms are selected using two criteria: random selection or based on the energetics of each atom (high energy atoms are displaced first).[75] The random selection of the atoms can be used with empirical and first-principles potentials, while the second approach can be applied only with empirical potentials as the decomposition of DFT total energies in atomic contributions is not a straightforward task. From our calculations, we found that S = 0.30–0.40, $\alpha_{\min}$ = 0.20–0.30, $\alpha_{\max}$ = 0.45–0.60, and w = 2, yield good results; however, those parameters can be optimized to yield optimum performance for most particle size and interaction model.

b. Twist Operator (TO) – Nonlocal. In contrast with local operators, TO was originally designed to produce large structural changes in the particle by rotating a set of atoms around a particular axis.[19] The particle is approximated as a sphere, and a random plane separates it into two portions with different sizes, with one of these portions subjected to a random rotation around the axis perpendicular to the sectioning plane. In our implementation, first, we apply a

dx.doi.org/10.1021/ci400224z | J. Chem. Inf. Model. 2013, 53, 2282–2298

random rotation defined by the matrix $R(\phi, \psi, \theta)$, where the angles are random numbers in the range $[0, 2\pi]$. Then, a random number in the range $[-R_{max}, R_{max}]$ is drawn and used to define a plane perpendicular to the z-axis, and therefore two portions are defined below and above the level given by this random number, and a random rotation, $[0, 2\pi]$, is performed on one of them.

c. Angular Operator (AO) – Nonlocal. This operator was first introduced by Wales and Doye,[20] and it has been probably overlooked by most studies employing BHMC, with few exceptions.[76] It works by selecting one or more atoms and randomly placing them over a sphere of radius equal to their distance to the geometric center of the particle, i.e., R_i for atom i. The selection of the atoms can be based either on random selection or on the energy contributions of the individual atoms. Our results indicate that AO is efficient to fill vacant sites in the particle, and the optimum number of selected atoms is in the range of 1% to 5% of the total number of atoms

d. Surface Angular Operator (SAO) – Nonlocal. The SAO selects an atom i randomly in the particle and places it in a random position on the particle surface, $R_{max}\hat{\mathbf{e}}_i(\theta_i, \phi_i)$.[77] Thus, it helps to fill vacant sites on the surface, and hence, it plays an important role for nearly spherical particles; however, the same does not hold for nonspherical particles.

e. Interior Operator (IO) – Nonlocal. In contrast with the SAO, which brings atoms to the particle surface, the IO moves atoms from the surface to the interior of the particle,[77,78] and therefore increases the chances of filling vacant sites in the core region. In our implementation, all N atoms are sorted according to their distances to the geometric center, and the operator selects the farthest atoms and places them in a small sphere centered at the geometric center of the particle, with radius about 1% to 10% of the particle radius, R_{max}. From our calculations, the optimum number of affected atoms depends on particle size and on the stability of the core region, and once the core region reaches its ground state energy this operator loses most of its efficiency.

f. Exchange Operator (EO) – Nonlocal. In particles with more than one chemical species, diffusion barriers add an extra difficulty in the identification of the ground state configuration as they limit the motion of the atoms. The EO randomly selects a set of pairs of atoms i and j of different chemical species α and β, respectively, and exchanges the species among the atoms of each pair, i.e., $(\mathbf{r}_i^\alpha, \mathbf{r}_j^\beta) \rightarrow (\mathbf{r}_i^\beta, \mathbf{r}_j^\alpha)$. The EO is a fundamental operator to obtain the putative global minimum structures for nanoalloys. For larger nanoalloys, specially those which are known to display core–shell structures, random exchanges may not be the most efficient strategy. Bochicchio and Ferrando[79] suggested the use of tailored exchanges specific to the system under investigation, in which the coordination number of each atom and the species of its neighbors are taken into account to guide the exchange procedure. In this work we did not follow this approach, since one of our goals is to keep the operators general and suitable to different classes of systems; however, it could be included in this set of operators if all others fail to yield the desired performance for nanoalloys.

g. Geometric Exchange Operator (GEO) – Nonlocal. In contrast with the exchange operator above that selects randomly the atoms i and j of each pair, the GEO picks an atom i at position $\mathbf{r}_i^\alpha$ located in the core region, satisfying the condition $R_i < (R_{max}/2)$, and another atom j at position $\mathbf{r}_j^\beta$ from the surface region, satisfying the condition $R_j > (R_{max}/2)$, and then exchanges the chemical species of both sites. This operator is efficient to move atoms from the core to the surface region, and vice versa; however, it is not efficient once the equilibrium composition is reached.

h. Crossover Operator – Nonlocal. This operator is based on the well-known mating crossover of two particles commonly used in GA.[19,80] In our BHMC implementation, we select two particles, parents $\{\mathbf{R}^A\}$ and $\{\mathbf{R}^B\}$, to perform the crossover and obtain two new particles, children $\{\mathbf{R}^{A'}\}$ and $\{\mathbf{R}^{B'}\}$, out of which only the one with lowest energy is kept. The particle $\{\mathbf{R}^A\}$ is obtained from the database of lowest energy configurations which are collected along the calculation, and $\{\mathbf{R}^B\}$ is the configuration accepted in the last application of the Metropolis selection criterion. This procedure aims to combine features of two different and already explored regions of the PES in order to lead to a third region, hopefully not yet explored. The Crossover operator is applied whenever a fixed number of BHMC steps have elapsed, e.g., from 50 to 1000 steps, which depends on the size of the particle. Three types of crossover techniques are available, namely one-point, two-point, and geometric crossover.[81]

i. Occasional Jump (OJ) – Nonlocal. This operator was introduced by Iwamatsu and Okabe[37] and was designed to avoid that a particular configuration, $\{\mathbf{R}\}$, gets trapped in a deep funnel-like minimum. It works by accepting a consecutive number of new configurations, $\{\mathbf{R}'\}$, independently of their energies with respect to the current one. This approach is equivalent to increasing the temperature of the Metropolis criterion to a very large value for a few BHMC steps. In our implementation, the OJ is activated only after a fixed number of consecutive rejections by the Metropolis criterion is reached considering all active trial operators. A particular trial operator may not be able to move a configuration out of a deep minimum; however, a different operator might be able to do it. Thus, it is important to provide the chance for all active trial operators to be applied before the OJ operator takes action. This operator is critical for low temperature BHMC calculations, e.g., nearly zero, which corresponds to a downhill exploration.

j. Auxiliary Filter Operator (AFO). All operators described above yield a new configuration, $\{\mathbf{R}'\}$, once an old configuration, $\{\mathbf{R}\}$, is provided. However, there is no constraint on the possible atomic position of the atoms in the resulting structure; therefore, configurations with atoms i and j very close to each other can occur, which can drastically affect the convergence of first-principles calculations, posing serious limitations for the BHMC-DFT technique. To address this issue we applied the same filter used for the randomly initialized configurations but now with a different parameter, $(1 - \eta)R_c^{\alpha\beta} < d_{ij} < (1 + \eta)R_c^{\alpha\beta}$, where η is the parameter controlling the tightness of the filter. All new configurations generated by any trial operator, $\{\mathbf{R}'\}$, are submitted to this auxiliary filter, which can either accept or reject them. If $\{\mathbf{R}'\}$ is rejected, then a new configuration is generated by the same trial operator; however, after a maximum number of consecutive rejections the algorithm moves on to the next trial operator, thus avoiding an infinite loop. At the end of Section III, the performance of this operator is provided and discussed.

The only trial operators that we classify as local are the simple atomic displacement operators, CDO and GCDO, which move the atoms around their original positions. The rest of the set is better termed nonlocal, since the atoms are in general moved to new atomic positions far away from their original positions. The exception is the AFO, which does not

change the input structure, serving only the purpose of accepting or rejecting a given structure based on structural considerations alone. The differences between local and nonlocal operators are illustrated in Figure 1. Local operators are able to explore a region which is nearby to the current search location, and surmounting high energy barriers or moving to farther regions through local operators takes several BHMC steps. Nonlocal operators, however, can guide the search to regions separated by large energy barriers in a small number of steps. We found that the efficiency of the BHMC algorithm can be enhanced by combining in an interposed way local and a diversity of nonlocal operators.

Using different operators together with BHMC is not a novel idea, as it can be seen in ref 75, by Rossi and Ferrando. Some of the operators from their paper bear resemblance to those we describe in this section. For example, their single and shake moves are similar to CDO, while SAO is very similar to the shell moves described in that reference. Moreover, Ferrando and co-workers[75,79,82] make use of high-temperature molecular dynamic runs as an operator within BHMC, which can show a significant improvement in performance for large particles in comparison with displacement operators such as CDO and GCDO.[79] In our strategy, however, we employ several different operators that allow a greater variety of structural changes and consequently a more thorough exploration of the PES with respect to operators sets described in other studies. In addition, we introduce the notion of local and nonlocal operators, which to our knowledge has not been explored in any of the previous studies cited.

4. Acceptance Rate. Certain values of acceptance rate for the Metropolis criterion have been commonly used as rule of thumb to allow a reasonable sampling of high dimensional PES[74,83] such as 0.234 and 0.50. Target values of the acceptance rate for a fixed temperature can be achieved by controlling the magnitude of $\Delta\mathbf{r}_i$ or the number of atoms that are displaced.[21] However, the use of a large number of trial operators with local and nonlocal structural features introduces a fundamental difficulty with regard to controlling the acceptance rate, given that the energy scale of different operators may be quite different. For example, an operator that acts on a single atom is more likely to produce a new configuration with a small energy difference compared with the old configuration, while an operator acting on several or all atoms may yield an output structure with a large energy difference with respect to the input structure. In this section we summarize our ideas to overcome this problem and take advantage of a large set of operators within the BHMC algorithm.

In our implementation, we use one of two different schemes to apply the trial operators, namely, a static and a dynamical one. In both schemes, a sequential list of interposed local and nonlocal trial operators is provided. The two schemes are based on the assumption that when a large set of operators is used, it is better to work around the acceptance rate issue by recognizing that different operators will not have the same efficiency and by prioritizing those which contribute more to the optimization. In the static scheme every operator is applied for a fixed number of steps, following the provided sequence. The number of applications of each operator can be different, and once the sequence is completed, the algorithm starts at the first operator again, so the sequence is used cyclically. In the dynamical scheme, each operator in the sequence is applied until it reaches a consecutive number of rejections by the Metropolis criterion. Once the sequence is completed, the algorithm cycles over it again, as in the static scheme.

The dynamical scheme is based on the idea that each operator should have the chance to act for a while before moving on the next operator. Thus, a trial operator that is not suitable for a system would be applied only a minimum number of times, while a suitable operator would be applied consecutively for several steps before moving to the next one in the sequence. For example, some trial operators that yield large structural changes can be very useful in the first steps but may lose their efficiency along of the optimization, while others may gain importance.

C. Interacting Potentials. *1. Empirical Potentials.* Both LJ and SC potentials have been widely discussed in the literature,[64,84] and here we present only their main features. The total energy of a system of N interacting atoms described by the LJ pair-potential is given by

$$E_{\mathrm{tot}}^{\mathrm{LJ}} = \frac{1}{2}\sum_{i=1}^{N}\sum_{j\neq i}^{N} 4\epsilon^{\alpha\beta}\left[\left(\frac{\sigma^{\alpha\beta}}{r_{ij}}\right)^{12} - \left(\frac{\sigma^{\alpha\beta}}{r_{ij}}\right)^{6}\right] \tag{5}$$

where $r_{ij} = |\mathbf{r}_j - \mathbf{r}_i|$, and $\epsilon^{\alpha\beta}$ and $\sigma^{\alpha\beta}$ are energy and length scaling parameters, respectively, that depend on the chemical species α and β of the pair of interacting atoms. In this work we employ reduced units for all LJ calculations, which is commonly used for LJ clusters.[20,85,86] In this case, $\epsilon^{\alpha\alpha} = \epsilon^{\beta\beta} = 1$, $\sigma^{\alpha\alpha} = 1$, $\sigma^{\beta\beta} = 1.05$ to 1.30 in steps of 0.05, and for interacting atoms of different species the combination rules used to determine the parameters are $\epsilon^{\alpha\beta} = (\epsilon^{\alpha\alpha}\epsilon^{\beta\beta})^{1/2}$ and $\sigma^{\alpha\beta} = (\sigma^{\alpha\alpha} + \sigma^{\beta\beta})/2$.

In the SC potential the total energy is given by

$$E_{\mathrm{tot}}^{\mathrm{SC}} = \sum_{i=1}^{N}\left(\frac{1}{2}\sum_{j\neq i}^{N} V_{ij} - c_i^{\alpha}\sqrt{\rho_i}\right) \tag{6}$$

where

$$V_{ij} = \epsilon^{\alpha\beta}\left(\frac{a^{\alpha\beta}}{r_{ij}}\right)^{n^{\alpha\beta}} \tag{7}$$

and

$$\rho_i = \sum_{j\neq i}^{N} U_{ij},\ U_{ij} = (\epsilon^{\alpha\beta})^2\left(\frac{a^{\alpha\beta}}{r_{ij}}\right)^{m^{\alpha\beta}} \tag{8}$$

The constants $\epsilon^{\alpha\beta}$, c_i^{α}, $a^{\alpha\beta}$, $n^{\alpha\beta}$, and $m^{\alpha\beta}$ have been parametrized for several systems using bulk reference data.[64,65] For single species SC particles we employed energy and length reduced units in our calculations, i.e., $\epsilon^{\alpha\alpha} = 1$, $a^{\alpha\alpha} = 1$. The other three parameters were set to the values for Rh and Ag bulk systems,[64] i.e., $c_i^{\alpha} = 144.41$, $n = 12$, $m = 6$, which is known as the 12−6 SC potential. For the binary $(AgPd)_{55}$ system, we used the parameters summarized in Table 1.[65] The rules for combining the parameters to describe interactions between atoms of different species are analogous to those used in the LJ case.

The forces between atoms are used by the local minimization procedure and can be found by taking the negative gradient of eqs 5 and 6. The force on atom i due to atom j for the LJ and the SC potentials are, respectively

Table 1. Sutton-Chen Parametrization for Pairs of Ag and Pd Atoms[65]

atom pair	n	m	c	ϵ (eV)	a (Å)
Pd−Pd	12	6	148.205	3.2864×10^{-3}	3.8813
Ag−Ag	11	6	96.524	3.9450×10^{-3}	4.0691
Ag−Pd	11.5	6	-	3.6007×10^{-3}	3.9752

$$\mathbf{F}_{ij}^{LJ} = -24\epsilon^{\alpha\beta}\left[2\left(\frac{\sigma^{\alpha\beta}}{r_{ij}}\right)^{12} - \left(\frac{\sigma^{\alpha\beta}}{r_{ij}}\right)^{6}\right]\frac{\mathbf{r}_{ij}}{r_{ij}^2} \quad (9)$$

and

$$\mathbf{F}_{ij}^{SC} = -\left[n^{\alpha\beta}V_{ij} - \frac{m^{\alpha\beta}}{2}\left(\frac{c_i^{\alpha}}{\sqrt{\rho_i}} + \frac{c_j^{\beta}}{\sqrt{\rho_j}}\right)U_{ij}\right]\frac{\mathbf{r}_{ij}}{r_{ij}^2} \quad (10)$$

In order to simplify the notation in the remaining of this text, we will drop the species superscripts of ϵ for both LJ and SC potentials. For example, for cases where $\epsilon^{\alpha\alpha} = \epsilon^{\beta\beta}$ or for single species particles. Moreover, in the cases where reduced units are used the energies will be given in units of ϵ.

2. First-Principles - Density Functional Theory. Our spin-polarized calculations are based on DFT[87,88] within the generalized gradient approximation (GGA) proposed by Perdew, Burke, and Ernzerhof[89] (PBE) for the exchange-correlation (xc) energy functional, as implemented in the all-electron full-potential electronic structure package FHI-aims.[73] This package employs contracted atomic orbitals to expand the Kohn−Sham orbitals and allows nonperiodic calculations, which is very convenient to study the physical and chemical properties of clusters and nanoparticles.[90]

In our BHMC calculations, we employed the default *light* settings with *tier1* basis set in FHI-aims, which provides enough accuracy to explore the PES of Al_N clusters (N = 2−30) at a reasonable computational cost. The Gaussian broadening parameter was set to 10^{-1} eV, the energy convergence to 10^{-4} eV, and the atoms considered at equilibrium positions once all atomic forces have magnitude less than 10^{-2} eV/Å. The ground state structures obtained by BHMC-DFT for Al_N were reoptimized using DFT-PBE with a high level basis set (*tight* settings with default *tier2* basis set), with a broadening parameter of 10^{-2} eV, energy convergence criterion of 10^{-5} eV, and the atoms at equilibrium once all forces have magnitude less than 10^{-3} eV/Å. The reference structures available in the literature[91] were also reoptimized using FHI-aims with these same settings in order to allow a fair comparison.

III. RESULTS

To evaluate the performance of our BHMC implementation, we applied it to the following systems: (a) LJ_N clusters (N = 2−147), (b) LJ_N NPs (N = 200, 250,···, 1000 1500), (c) SC_N clusters (N = 3−148), (d) BLJ_N clusters (N = 5−100), (e) binary transition-metal $(AgPd)_{55}$ clusters described by the SC potential,[64,65] and (f) Al_N clusters (N = 2−30) described within DFT-PBE. Therefore, we performed BHMC optimization for about 960 different particles spreading from small to large sizes and different interacting potentials.

All BHMC runs started with one randomly initialized structure following the procedure given in Section II B 1, and the most important BHMC parameters are summarized in Table 2. From preliminary tests, the Crossover operator proved to be efficient only for LJ NPs, while the OJ operator was most useful for binary systems optimized at low temperatures. The temperatures were fixed at values which allowed a good exploration of the PES for each particular class of systems, and no systematic effort was put into finding the optimum temperature for any particular systems. The determination of the order of operators was also empirical and driven by results from preliminary tests, and the ordering shown in Table 2 should not be taken as definite, the important factor here being the interposing of local and nonlocal operators.

Except for the DFT calculations, in all other cases the dynamic scheme was used for the operators. For low temperatures (e.g., k_BT = 0.1 reduced units) we recommend a rejection limit of 10 to 20, while for higher temperatures (e.g., k_BT = 1.6 reduced units) lower rejection rates seem to be optimal, ranging from 2 to 5 rejections. The strategy that we recommend is to allow the local operators a higher rejection rate than the nonlocal operators, such as twice the number of rejections. For the DFT calculations the static scheme was employed, in which the local and nonlocal operators were applied for 15 and 8 consecutive steps, respectively. The overall success rate should improve if the temperature and the operators parameters are further optimized for each class of system; however, we did not put a great effort in this task. The fact that we were able to obtain good results for all cases considered even with different order of operators and different sets of parameters show that the method is general and not extremely sensitive to these settings, although better results can be achieved with an optimal setup.

The total number of BHMC steps varied among different systems, depending on the interaction potential considered and particle size. For LJ and SC potentials the number of steps varied from 10^2 to 10^5. For BHMC-DFT calculations, in which the computational cost is several orders of magnitude higher than interacting LJ and SC potentials, we performed a

Table 2. BHMC Parameter Settings[a]

class of systems	k_BT	OJ	Crossover	operators
LJ_N (N = 2−147)	1.6	no	no	GCDO, TO, CDO, SAO, GCDO, AO, CDO, IO
LJ_N (N = 200,...,1500)	1.6	no	yes (1000)	GCDO, TO, CDO, SAO, GCDO, AO, CDO, IO
SC_N (N = 3−148)	1.6	no	no	GCDO, SAO, CDO, TO, GDO, AO, CDO, IO
BLJ_N (N = 5−100)	0.1	yes (4, 2500)	no	CDO, TO, GCDO, AO, EO, SAO, GCDO, IO, GEO
SC $(AgPd)_{55}$	0.1	yes (3, 1000)	no	CDO, SAO, TO, EO, AO, GCDO, IO, GEO
DFT Al_N (N = 2−30)	0.1−0.2	no	no	GCDO, TO, AO, CDO, SAO

[a]For occasional jumping (OJ) the number of jumps and how many rejections to wait before jumping are enclosed in parentheses. For Crossover the number enclosed in parentheses indicates the amount of MC steps between consecutive applications of the operator. The operators are arranged in order of usage during the BHMC runs, according to the naming conventions defined in Section II B 3.

maximum of 1500 BHMC steps, which we believe to be enough to obtain accurate ground state structures for most of the Al_N clusters (N = 2−30). The analysis of the point group symmetries, which is important for comparison with previous results, was performed using the OPTIM package.[92]

A. LJ_N Clusters. The global minima found in this work for LJ_N clusters (N = 2−147) are in complete agreement with the putative global minima available in the literature, collected in the Cambridge Cluster Database.[93] As found in previous studies,[20,86,94−100] we identified the complete Mackay icosahedron for LJ_{13}, LJ_{55}, and LJ_{147}, while truncated octahedron were found for LJ_{38}, LJ_{79}, LJ_{116}, and LJ_{140}, Leary tetrahedron[100] is the geometry of LJ_{98}. For LJ_{75-77} and $LJ_{102-104}$ the most stable structures present geometries based on Marks decahedron.[101]

We performed 100 independent BHMC runs for a few selected systems, namely LJ_{38}, LJ_{75}, and LJ_{98}, which correspond to multiple funnel systems and are considered among the most difficult cases in the range considered here and also for the single funnel system LJ_{55}, a relatively easy case for global optimization. All runs started from a single randomly initialized structure and were allowed to continue until the global minimum was found for each case, which means that a 100% success rate was achieved in every case. Two sets of 100 runs were performed for each system, one employing the static scheme of applying the operators, while the other employed the dynamic scheme. In all cases the mean first encounter time (MFET) was calculated, which is simply the average number of steps required to locate the global minimum, and in the case of BHMC corresponds to the number of local minimizations, since in BHMC one local minimization is carried out in each step. Our results are summarized in Table 3, in which we compare them with the most recent BHMC results available for LJ clusters.[48]

Table 3. Mean First Encounter Times Calculated from 100 Independent Successful BHMC Runs for Selected Sizes of LJ_N Clusters Using the Static and Dynamic Schemes of Operators (First and Second Columns, Respectively)[a]

N	static scheme	dynamic scheme	traditional BHMC[48]	symmetrized BHMC[48]
38	1045	647	1271	34
55	79	77	92	103
75	78161	60583	61668	338
98	8365	7413	48301	563

[a]Recent reference results are shown for comparison (third and fourth columns).[48].

In all four cases the dynamic scheme of operators proved to be more efficient than the static scheme; however, the differences are only modest, except for LJ_{75}. Using the dynamic scheme we were able to obtain lower MFETs than those reported in ref 48 using a traditional BHMC algorithm, with a more pronounced difference for LJ_{98}, in which case our implementation using the dynamic scheme was able to locate the global minimum in about 40000 steps less. However, the symmetrized BHMC exploring the PES with a symmetry bias,[48] but without favoring any particular point group, still performs better than our implementation by 1 to 2 orders of magnitude. These results seem to confirm that an exploration based on random structural operators is outperformed by searches which are symmetry-driven and take advantage of a maximum symmetry principle, derived mostly empirically from the observation that global minima for LJ clusters are more probable to have higher symmetries than other low-lying isomers, or at least higher approximate symmetries, as observed by Oakley et al.[48]

Furthermore, our implementation should allow a 100% success rate for all cases of LJ_N clusters (N = 2−147) within a reasonable number of steps. This can be compared with previous studies, e.g., Locatelli and Schoen[35] were able to obtain a 94% success rate in locating the global minimum of LJ_{75} using a two-phase local optimization, and only 0.80% using a BH algorithm, while here we report 100%.

B. LJ_N Nanoparticles. From our knowledge, there is no systematic investigation of LJ_N NPs (N > 250) using BHMC, even though different global optimization algorithms have recently addressed the study of large LJ_N particles.[102−105] In this work we applied our BHMC implementation to the following LJ_N NPs, N = 200, 250, 300, 350, 400, 450, 500, 1000, 1500. The total energies are summarized in Table 4 along with previous results for comparison. For each size we performed 100 BHMC runs of 50000 steps each.

Table 4. Total Energies for LJ_N NPs (N = 200,...,1500) Determined with Our BHMC Implementation Compared with Reference Data[g]

N	reference E_{tot}^{LJ} (ϵ)	this work E_{tot}^{LJ} (ϵ)	total error (%)
200	−1229.184776[a]	−1229.184776	0
250	−1579.794975[b]	−1579.794975	0
300	−1942.106775[a]	−1942.106775	0
350	−2293.181867[c]	−2293.181867	0
400	−2651.675335[c]	−2651.675335	0
450	−3015.164293[c]	−3015.164293	0
500	−3382.693487[d]	−3382.693487	0
1000	−7128.821829[e]	−7119.993439	0.12
1500	−10962.585028[f]	−10932.433410	0.28

[a]Reference 106. [b]Reference 107. [c]Reference 102. [d]Reference 108. [e]Reference 103. [f]Reference 104. [g]For $N \leq 500$ the putative global minima were located.

For $N \leq 500$ the total energies of the global minima are in complete agreement with previous results. The global minima for LJ_{200}, LJ_{250}, LJ_{300}, and LJ_{350} were located in at least two runs in less than 20000 steps, while for LJ_{400}, LJ_{450}, and LJ_{500} only one run for each case succeeded in finding the global minima previously reported.[102,106−108] In other cases, LJ_{1000} and LJ_{1500}, our final structures have higher energies than reference data,[103,104] with relative differences in total energy of 0.12% and 0.28%, respectively, increasing as the number of atoms is increased. We would like to stress that our calculations start from completely unbiased structures, and hence, we believe that our implementation provides a route to perform unbiased study of large particles.

The structures found in this work for the cases that BHMC failed to find the putative global minima present some ordering and planar faces, despite not having any symmetry, given that the structures that we located belong to point group C_1. The putative global minimum reported by other authors have icosahedral motif[102,103] for LJ_{1000} and a motif based on Marks decahedron[101,104] for LJ_{1500}. A closer inspection of our structures reveals that the underlying motifs are present; however, our structures are less compact in some regions, presenting vacancies and groups of surface atoms sticking out. To our best knowledge, no unbiased global optimization

dx.doi.org/10.1021/ci400224z | J. Chem. Inf. Model. 2013, 53, 2282−2298

Table 5. Energies and Point Group (PG) Symmetries for the SC_N Clusters (N = 81−148)

N	energy (ϵ)	PG	N	energy (ϵ)	PG	N	energy (ϵ)	PG
81	−79387.8066	C_s	104	−103649.9534	C_{2v}	127	−127734.1834	C_s
82	−80447.8861	C_s	105	−104635.8467	C_s	128	−128822.8084	C_1
83	−81496.0015	C_{2v}	106	−105688.1268	C_1	129	−129900.0012	C_s
84	−82549.7178	C_s	107	−106740.5143	C_{2v}	130	−130945.4633	C_1
85	−83567.9388	C_s	108	−107858.3157	C_s	131	−132064.2300	C_{2v}
86	−84650.1108	C_s	109	−108842.6864	C_s	132	−133082.8459	C_s
87	−85700.4419	C_s	110	−109901.9289	C_1	133	−134102.6010	C_1
88	−86698.6229	C_1	111	−110957.4546	C_1	134	−135184.3688	C_{3v}
89	−87782.6574	C_{3v}	112	−112049.4453	C_s	135	−136297.7226	C_s
90	−88793.5148	C_1	113	−113152.7706	C_{2v}	136	−137387.0536	C_s
91	−89911.5273	C_{3v}	114	−114133.5363	C_s	137	−138488.2876	C_{3v}
92	−90899.2953	C_1	115	−115191.0000	C_1	138	−139518.7051	C_{3v}
93	−91957.1142	C_1	116	−116271.2648	C_{3v}	139	−140620.0856	C_{2v}
94	−93046.3936	C_s	117	−117360.6586	C_s	140	−141721.4124	C_s
95	−94148.7083	C_{2v}	118	−118345.0657	C_s	141	−142822.8554	C_{5v}
96	−95128.9315	C_s	119	−119404.3767	C_1	142	−143923.9871	C_s
97	−96185.7908	C_1	120	−120467.7085	C_{2v}	143	−145025.2322	C_{2v}
98	−97261.2225	C_s	121	−121552.3108	C_s	144	−146126.4115	C_{3v}
99	−98363.7087	C_s	122	−122655.8679	C_{2v}	145	−147227.5242	C_{2v}
100	−99456.3734	C_{5v}	123	−123541.9028	C_1	146	−148328.7496	C_{5v}
101	−100559.4244	D_{5h}	124	−124626.0202	C_s	147	−149430.0837	I_h
102	−101540.5033	C_{2v}	125	−125746.3797	C_s	148	−150308.0658	C_s
103	−102597.7356	C_s	126	−126679.9830	C_1			

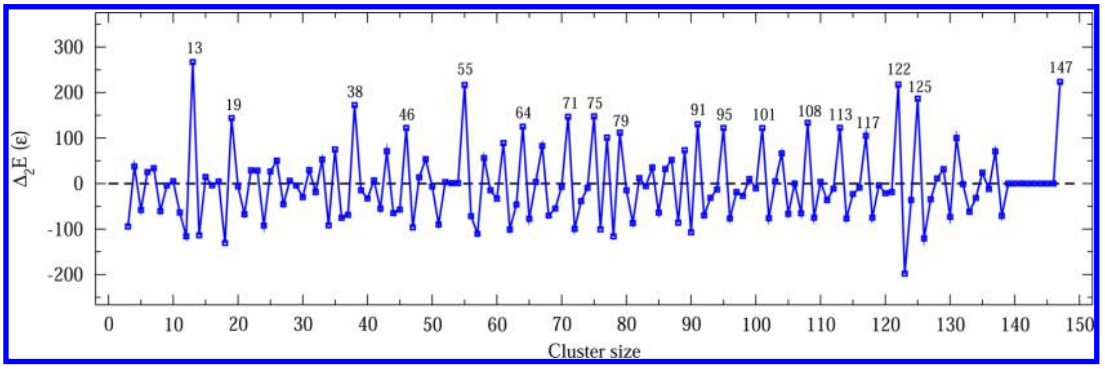

Figure 3. Second energy difference (relative stability) of the 12−6 SC_N clusters (N = 3−147).

method has succeeded in locating the putative global minima of LJ_{1500} thus far. Nevertheless, for LJ_{1000} Goedecker[109] reports success in locating the global minimum using an unbiased minima hopping algorithm based on molecular dynamics after evaluating a few million configurations.

C. SC_N Clusters. For the case of SC_N clusters (N = 3−148), we employed the 12−6 SC empirical potential in reduced units, and several runs were performed for each system. The global minimum structures found in the range N = 3−80 as well as their corresponding energies and symmetries are in complete agreement with previous results.[33,93] To our knowledge no previous investigations have been reported for N = 81−148, and the results for this range are summarized in Table 5.

The second energy difference for a cluster of size N is defined as $\Delta_2E(N) = E_{tot}(N + 1) + E_{tot}(N - 1) - 2E_{tot}(N)$ and measures the relative stability of the cluster with respect to neighboring sizes. The relative stability of the SC_N (N = 3−147) clusters are shown in Figure 3, and it follows a similar pattern found by Grigoryan et al.[110] for Cu_N clusters (N = 2−150) described by an embedded-atom method. In the range N = 3−80, Figure 3 is identical to the one published by Doye and Wales,[33] which clearly indicates the quality of our data. For N > 80 there are more structures presenting relatively high stability in comparison with the range $N \leq 80$. The structures with high stability are found at N = 91, 95, 101, 108, 113, 117, 122, 125, and 147, with the most pronounced peaks at N = 122, 125, and 147. Some high symmetric clusters, e.g., SC_{101} and SC_{147}, have high relative stability, but overall it appears that no correlation can be established between the point group symmetry of the particles and their relative stability.

D. Binary LJ_N Clusters. Several studies focused on the global optimization of BLJ clusters,[77,111−115] making them a suitable benchmark to test our implementation. We performed calculations for N = 5−100 atoms using fixed compositions, i.e., the number of atoms of each species for a particular size was kept constant, as our goal here is to evaluate our BHMC strategies and not to perform a thorough study of these clusters. The compositions employed here, N_A and N_B, are those reported by Doye and Meyer[112] and available in the Cluster Cambridge Database.[93] The two atomic species are made different by using different values for the ratio σ^{BB}/σ^{AA}, as described in Section II C. In order to be fair to previously published data, we collected in a single set the best results of all

studies[77,111−115] with the same compositions reported by Doye and Meyer[112] and compared our results against this set.

In Table 6 we show the results for the cases in which our BHMC implementation identified structures with lower global minimum energy relative to the reference compositions and structures from the set mentioned above. The putative global minimum structure identified in this work for BLJ_{38} (N_{AA} = 8, N_{BB} = 30, σ_{BB}/σ_{AA} = 1.05) has tetrahedral symmetry, belonging to point group T_d, and is 0.051613ϵ lower in energy than the previously known putative global minimum,[112] which has bilateral symmetry (point group C_s). To our best knowledge this is the lowest energy structure ever reported for BLJ_{38} for this value of σ_{BB}/σ_{AA}.

Table 6. BLJ_N Clusters (N = 5−100) Located with Our BHMC Implementation with Lower Energy Relative to the Best Known Structures[77,111−115] Using the Compositions As Reported by Doye and Meyer[112]

N	N_A	N_B	σ^{BB}/σ^{AA}	$E_{tot} - E_{tot}^{ref}$ (ϵ)	PG	PG^{ref}
31	6	25	1.05	−0.016397	C_s	C_1
36	8	28	1.05	−0.007331	C_1	C_s
38	8	30	1.05	−0.051613	T_d	C_s
43	9	34	1.05	−0.197553	C_1	C_1
90	31	59	1.05	−0.216358	C_1	C_s
97	34	63	1.05	−0.292010	C_1	C_1
46	12	34	1.10	−0.021177	C_1	C_1
47	13	34	1.10	−0.013075	C_s	C_s
63	14	49	1.10	−0.266481	C_1	C_1
64	14	50	1.10	−0.203841	C_1	C_s
65	15	50	1.10	−0.109876	C_s	C_1
66	14	52	1.10	−0.227975	C_s	C_1
73	19	54	1.10	−0.853502	C_{3v}	C_s
76	21	55	1.10	−0.043272	C_1	C_1
77	23	54	1.10	−0.095686	C_1	C_1
83	25	58	1.10	−0.377999	C_1	C_1
84	25	59	1.10	−0.530894	C_1	C_1
85	25	60	1.10	−0.369416	C_1	C_1
86	25	61	1.10	−0.581781	C_1	C_1
64	19	45	1.15	−0.427895	C_2	C_1
66	20	46	1.15	−0.000003	C_s	C_s
74	24	50	1.15	−0.074097	C_1	C_1
80	25	55	1.15	−0.299893	C_1	C_1
81	26	55	1.15	−0.125538	C_s	C_s
90	27	63	1.15	−1.018939	C_s	C_1
91	27	64	1.15	−0.250191	C_s	C_s
92	30	62	1.15	−0.077081	C_2	C_{2h}
93	30	63	1.15	−0.056132	C_1	C_1
94	30	64	1.15	−0.455720	C_1	C_1

For the remaining BLJ systems not shown in Table 6, we found the exact same results for all systems as previously reported;[77,111−115] however, there were two exceptions, namely BLJ_{99} and BLJ_{100} (σ^{BB}/σ^{AA} = 1.30), for which the lowest reported reduced energies[114,115] are −597.592233ϵ and −604.796307ϵ, respectively, while we found −597.350577ϵ and −604.233674ϵ. Nevertheless, the structures that we found have lower energy in comparison with those found by Doye and Meyer[112] using BHMC, in particular 1.253040ϵ and 1.948576ϵ lower for BLJ_{99} and BLJ_{100}, respectively. Even though the differences with respect to the best available data in the literature for these two cases are small (relative errors of 0.40% and 0.93%, respectively), the structures are quite different. We found structures which are roughly spherical, whereas those from the literature are very close to prolate spheroids with large polar axis. For both cases we performed around 10000 calculations of 80000 BHMC steps each; however, the putative global minima reported in refs 114, 115 could not be found. We attribute this to the fact that our trial operators do not favor very pronounced prolate structures.

E. Binary SC - $(AgPd)_{55}$ Clusters. In the case of binary clusters described by the SC potential, we selected the $Ag_{55-n}Pd_n$ system with compositions from n = 0 (pure Ag) to n = 55 (pure Pd) in steps of unit, and at each composition we performed 100 independent BHMC runs of 100000 steps each. The excess energy, E_{exc}, which measures the relative stability of the alloy with respect to the pure phases, is defined as

$$E_{exc} = E_{tot}(Ag_{55-n}Pd_n) - \left[\frac{(55-n)}{55}E_{tot}^{Ag} + \frac{n}{55}E_{tot}^{Pd}\right] \quad (11)$$

where $E_{tot}(Ag_{55-n}Pd_n)$ is the total energy of $Ag_{55-n}Pd_n$, while E_{tot}^{Ag} and E_{tot}^{Pd} are the total energies of the Ag_{55} and Pd_{55} systems, respectively. The excess energy results are shown in Figure 4 along with the atomic structure for a few selected compositions.

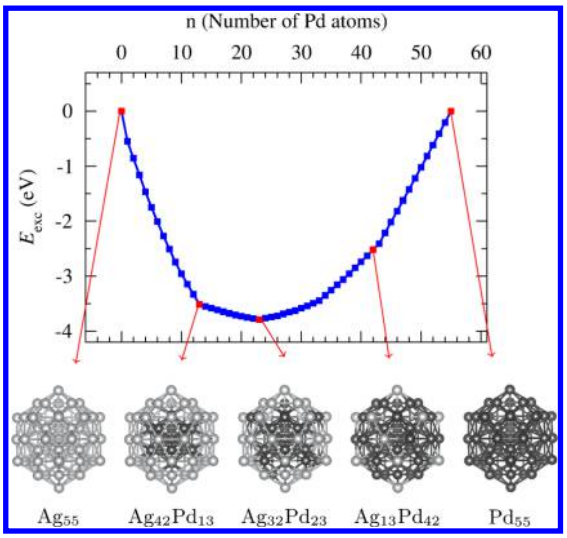

Figure 4. Excess energy of the binary $Ag_{55-n}Pd_n$ SC clusters as a function of Pd composition (n). For selected compositions, the structures are illustrated.

The position of the minimum of the excess energy curve indicates that $Ag_{32}Pd_{23}$ is the most stable composition, and therefore a Ag rich phase is favored. As the Pd composition is decreased, the Ag atoms prefer to occupy surface sites due to their larger radius compared with the Pd atoms. At n = 13 it is observed a dealloyed structure, with Pd atoms in the core and Ag atoms on the surface. As the number of Ag atoms increases, they tend to migrate to the inner layer and finally at n = 1 the only Pd atom remaining sits at the center.

In the case of $Ag_{42}Pd_{13}$, there are results reported in the literature from a simpler BHMC algorithm; therefore, making it a good candidate for assessing the performance of our approach.[68] In this case we found the core−shell icosahedron structure with total energy −150.99 eV, which is 0.58 eV lower than previously reported by Kim et al.[68] They were able to obtain the core−shell icosahedron structure as well, and this energy difference may be attributed to the fine differences in

dx.doi.org/10.1021/ci400224z | J. Chem. Inf. Model. 2013, 53, 2282−2298

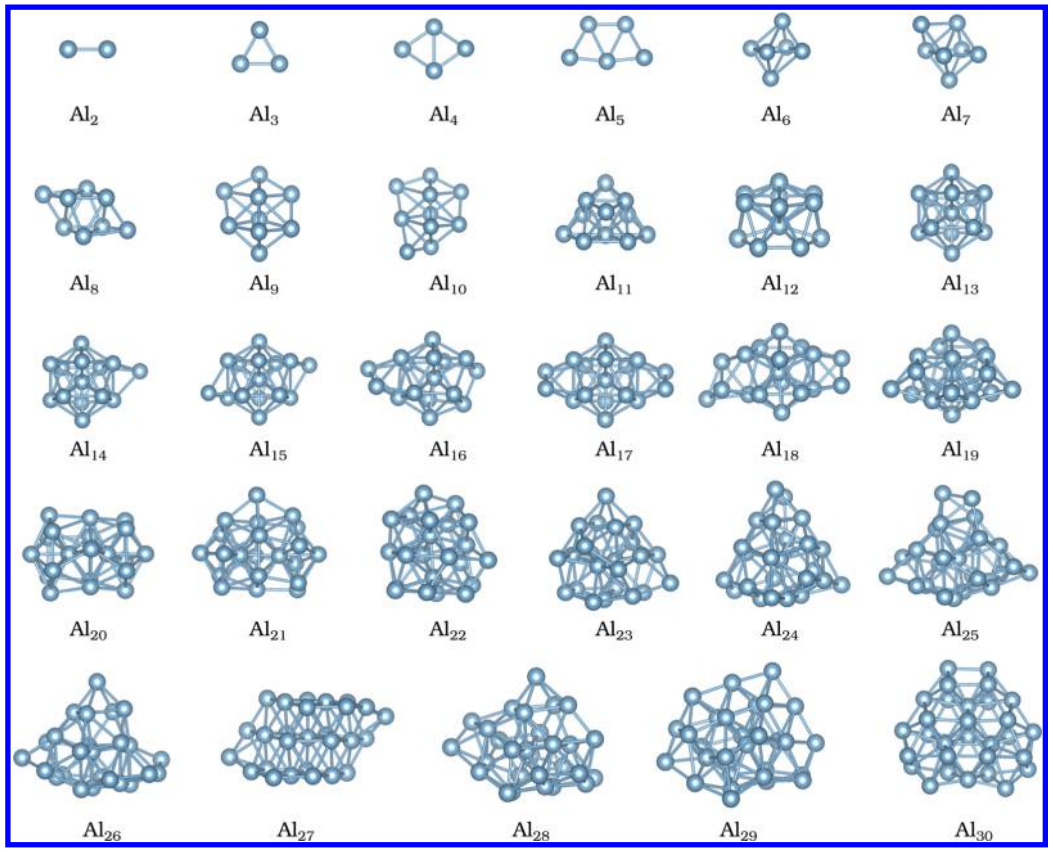

Figure 5. Lowest energy Al_N clusters (N = 2−30) configurations found with our BHMC-DFT calculations. The images were generated using the Visualization for Electronic and Structural Analysis (VESTA) tool.[118]

the local optimization procedures employed in both studies. An effective coordination number[116] (ECN) analysis applied to the global minimum structure of $Ag_{42}Pd_{13}$ reveals that the central Pd atom and the 12 Pd atoms on the first layer have ECNs of 12.00 and 11.93, respectively. As for the Ag atoms, 12 of them are placed at the vertexes of the icosahedral motif with ECN of 5.96, while the remaining 30 atoms have ECN of 7.95. The atoms over the faces have a higher ECN than those at the vertexes as they are more closely packed. The ECN analysis reveals the perfect icosahedral symmetry of the $Ag_{42}Pd_{13}$ structure described by the SC potential.

Moreover, for each composition considered we found the same putative global minima in each of the 100 runs performed, and thus the success rate was 100% for all compositions. In particular, for $Ag_{42}Pd_{13}$ this rate can be compared with the 18.3% success rate reported by Kim et al.,[68] and on average we were able to find the global minimum for the first time (MFET) in 3050 BHMC steps, compared to 5829 BHMC steps reported by those authors. These results indicate that our approach leads to a higher efficiency in this particular case.

F. Al_N Clusters - DFT. Our BHMC implementation was combined with the electronic structure package FHI-aims[73] and applied to Al_N clusters (N = 2−30) following the same approach that we used for LJ and SC systems. In this case, at each size we performed one BHMC run with 1500 steps. The final structures found with BHMC-DFT can be seen in Figure 5.

A transition from planar to three-dimensional structure is verified from Al_4 to Al_5. As size increases the structures tend to get more tightly packed, and for Al_{13} a closed icosahedral structure is found, with a slight Jahn−Teller distortion reducing its symmetry from point group I_h to D_{3d}. There is a debate on whether the Al_{13} ground state structure is an icosahedron or decahedron. As Aguado and López[117] observed, a small group of theoretical studies points to the decahedron as the most stable structure, while many others identify the icosahedron (see ref 117 and references therein). Using the decahedron structure made available by Aguado and López we performed DFT-PBE calculations and found that it lies 0.29 eV higher in total energy than the icosahedron found with our BHMC-DFT calculations. Moreover, from Al_{14} up to Al_{19} it becomes clear that the underlying motif is based on the icosahedral Al_{13}.

We compared our final structures with the most recent putative global minimum available in the literature obtained from theoretical studies by Drebov and Ahlrichs,[91] and the summary can be seen in Table 7. In this comparison we considered two structures as degenerated if the energy difference between them was lower than 1 meV/atom, due to the precision allowed by basis set employed in FHI-aims.

With respect to total energy, our results agree with previously known structures in most of the cases. Our Al_{24} cluster is 0.094 eV lower in total energy (3.92 meV/atom) than the one previously reported,[91] and from our knowledge this is the first time that this structure has ever been reported. For Al_{23}, Al_{26}, Al_{27}, Al_{28}, and Al_{30} we were unable to match the putative global minima reported by Drebov and Ahlrichs;[91] however, the energy differences are relatively small. Moreover, we started from completely random structures and used only BHMC to perform the global optimization, while those authors employed a multistage optimization approach combining BHMC and GA. In our judgment, the fact that our BHMC implementation was able to find results that agree well with structures found with a

dx.doi.org/10.1021/ci400224z | J. Chem. Inf. Model. 2013, 53, 2282−2298

Table 7. Comparison of our Structures Found with BHMC-DFT with the Most Recent Global Minima Structures from Drebov and Ahlrichs[91a]

N	ΔE (eV)	ΔE (meV/N)	PG	PG^{ref}
2	-	-	$D_{\infty h}$	-
3	-	-	D_{3h}	-
4	-	-	D_{2h}	-
5	0.00014	0.03	C_{2v}	C_{2v}
6	0.00004	0.01	D_{3d}	D_{3d}
7	−0.00003	−0.01	C_{3v}	C_{3v}
8	0.00008	0.01	C_{2h}	C_{2h}
9	0.00014	0.02	C_s	C_s
10	0.00018	0.02	C_s	C_s
11	0.00049	0.04	C_{2v}	C_{2v}
12	0.00874	0.73	C_s	C_1
13	0.00010	0.01	D_{3d}	D_{3d}
14	−0.00004	−0.01	C_{3v}	C_{3v}
15	0.00031	0.02	C_{2h}	C_{2h}
16	0.00013	0.01	C_s	C_s
17	0.00010	0.01	D_{2h}	D_{2h}
18	0.00017	0.01	C_s	C_s
19	0.00097	0.05	C_1	C_1
20	0.00013	0.01	C_1	C_s
21	0.00026	0.01	C_s	C_s
22	0.00007	0.01	C_1	C_1
23	0.08765	3.81	C_1	C_{3v}
24	−0.09409	−3.92	C_1	C_1
25	0.00096	0.04	C_2	C_2
26	0.08931	3.44	C_1	C_1
27	0.35435	13.12	C_2	C_s
28	0.22989	8.21	C_1	C_{2v}
29	0.01397	0.48	C_1	C_{2v}
30	0.05557	1.85	C_2	C_1

[a]For sizes available for comparison the energy differences, $\Delta E = E_{tot}^{BHMC\text{-}DFT} - E_{tot}^{Ref}$, and point group (PG) symmetries are shown.

combination of techniques is a strong point in favor of our methodology.

In Figure 6 we show properties of the structures found in this work and also properties of the reference structures for comparison.[91] These properties are the stability curve defined by the second energy difference (Δ_2E), binding energy per atom, average ECN, average weighted bond length (d_{av}), total magnetic moment (m_{tot}), and HOMO−LUMO energy gap ($E_{HOMO-LUMO}$). The peaks at Al_7, Al_{13}, and Al_{20} in the second energy difference indicate that these structures are the most stable with respect to neighboring sizes and represent magic number clusters. No general evident correlation can be established between the stability curve and the other properties; however, for Al_7, Al_{13}, and Al_{20} it is possible to notice slightly higher values of E_b, ECN, and d_{av} with respect to neighboring sizes, making the curvatures of these curves negative at those points. The binding energy and average bond length of Al_{30} are 2.46 eV and 2.69 Å, respectively, still well below the experimental[84,119] bulk cohesive energy of 3.39 eV and lattice parameter of 4.05 Å, and therefore the convergence of these properties toward bulk values is very slow.

Cox et al.[120] probed the magnetic properties of aluminum clusters with up to 25 atoms using Stern-Gerlach deflection measurements; however, due to experimental limitations they were only able to determine the spin multiplicity for clusters with up to 10 atoms. According to that experiment, odd-atom

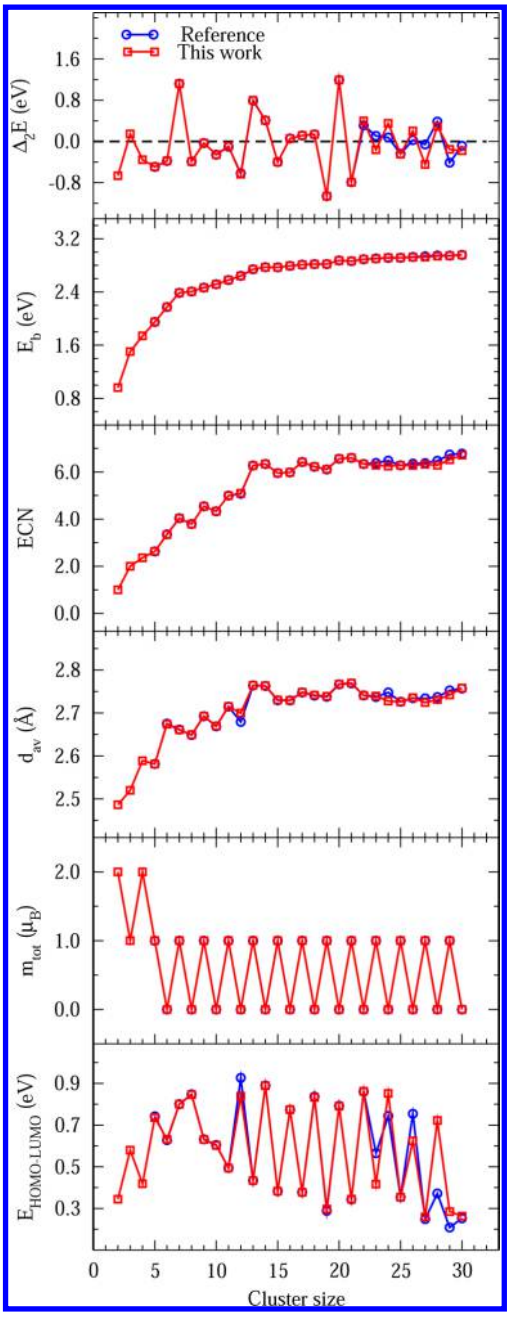

Figure 6. Properties of Al_N clusters (N = 2−30) found with BHMC-DFT (empty squares) compared with DFT-PBE results of reference structures (empty circles).[91] From top to bottom, second energy difference (Δ_2E), binding energy per atom (E_b), average effective coordination number (ECN), average weighted bond length (d_{av}), total magnetic moment (m_{tot}), and HOMO−LUMO energy gap ($E_{HOMO-LUMO}$), respectively.

clusters have a total magnetic moment of 1 μ_B, corresponding to doublet ground states, while even-atom clusters possess a total magnetic moment of either 0 μ_B or 2 μ_B, corresponding to either singlet or triplet ground states, respectively. The ground states found in our BHMC-DFT calculations agree with experimental data in all cases except for Al_6 and Al_8, for which experiments indicate that these are most likely triplets, while we found singlets. For these two cases we performed further DFT-PBE calculations on the BHMC-DFT structures fixing the cluster net spin to 2 and verified that the triplet

dx.doi.org/10.1021/ci400224z | J. Chem. Inf. Model. 2013, 53, 2282−2298

ground state of Al_6 lies 0.007 eV lower than the singlet, or 1.15 meV per atom, so the singlet and triplet are almost degenerated. For Al_8, however, the triplet ground state lies 0.19 eV higher than the singlet, or 23.24 meV/atom, and even though the difference is small, under our degeneracy criterion they correspond to nondegenerate states. We performed the same additional DFT-PBE calculations with the reference structures[91] as well and found the same results, as expected, since the reference structures are identical to ours for Al_6 and Al_8.

For sizes that our calculations were not able to identify the reference results, there are not very pronounced differences in the properties, and, in general, the same trends are observed, specially in the stability curve and in the HOMO−LUMO energy gap. From Al_{11} to Al_{19} the gap profile is consistent with an odd−even alternating behavior, where even-atom clusters present higher gaps with respect to neighboring sizes, which can be explained by closed electronic shells.[121] The most interesting difference is the energy gap difference between our result for Al_{28} and the reference structure. The higher energy gap of our structure indicates that it would be less reactive and thus have increased stability.

G. Filter Operator Analysis. In order to exemplify how the AFO described in Section II works, we performed one BHMC-DFT run on a randomly initialized Al_{15} cluster for 350 BHMC steps with the filter disabled. The static operators scheme was employed, and the trial operators used in this run were the same as shown in Table 2 for Al_N (N = 2−30), in the same order, with each operator set to act for 10 BHMC steps before proceeding to the next one. The 350 trial structures generated, i.e., each structure produced by the operators along the run, were collected, and afterward the AFO was applied to each one of them for two different values of the filter parameter, η = 0.2 and η = 0.4, the former corresponding to a tighter filter setting and the latter to a more relaxed one.

The results are shown in Figure 7, in which the collected structures were sorted in ascending order according to the computational time required by each corresponding DFT calculation (upper and middle panels). This timing corresponds to our BHMC-DFT implementations executing on a 16-core Intel Xeon processor model X5560 at 2.80 GHz. The difference between the energy of a structure produced in step s with respect to the lowest energy identified during the run, $\Delta E(s) = E_s - E_{lowest}$, is also shown in Figure 7 (lower panel).

In the upper and middle panels of Figure 7 the structures that would have been rejected by the filter during the run, if it was enabled, are marked with red filled circles. As it can be clearly seen, there is a correlation between the structures affected by the filter and the computational time. Those that require more time during a DFT calculation are the ones which are more likely to be rejected by the filter, indicating that these structures are more time-consuming because they have atoms too close to each other or too far apart, which the filter is able to detect. For η = 0.2, if the filter was enabled, it would have rejected 84.6% of the structures, corresponding to 94.4% of the total time necessary to perform DFT calculations on all 350 structures. With η = 0.4, the overall rejection rate would have been 28.3%, corresponding to 40.2% of the total computational time. These results show that the AFO is able to reduce the total computational time by avoiding costly DFT calculations on certain structures.

One might ask if the filter does not preclude BHMC from sampling a different variety of structures during the optimization. This question can be answered by an inspection of ΔE in the lower panel of Figure 7. The noise aspect of ΔE tells us that even if only a reasonable number of less time-consuming structures is considered, there is still a good variety of samples with respect to their relative energies. Hence there appears to exist no reason to perform the more expensive calculations, since they yield results which are potentially as good as those obtained in less costly calculations. In this case, η = 0.4 is a better choice. As a rule of thumb, the parameter η should be set within the range 0.3−0.5; however, an optimal value is system dependent.

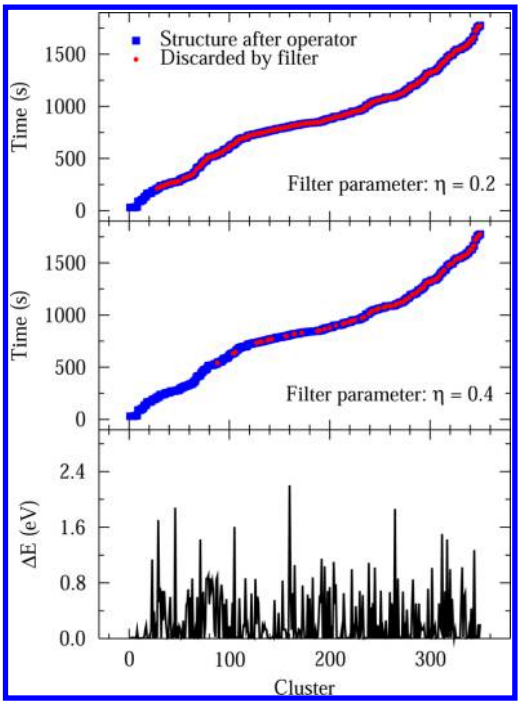

Figure 7. Structures collected along 350 BHMC steps of a BHMC-DFT run for Al_{15} with the auxiliary filter operator disabled. The structures are sorted in ascending order of computational time required by DFT calculations for each structure (filled blue squares, upper and middle panels). Structures that would have been rejected by the auxiliary filter operator are marked with filled red circles. In the lower panel the energy difference between each structure and the most stable one identified along the run is shown (ΔE).

The AFO also serves the purpose of avoiding DFT calculations on structures that are likely to result in problems in the electron density self-consistency. In such cases the calculations tend to take a long time before presenting convergence failure, consisting of a wasted computational effort. In the case of Al_{15}, during the run with the filter disabled there was a total of 14 out of the 350 BHMC steps in which the DFT calculations failed. The run was set up in a way that if a DFT calculation failed in a given step the step was restarted, so all 350 steps completed. When the AFO is enabled, self-consistency convergence problems are very seldom.

We performed a second run for Al_{15} using the same parameters of the first run described above, i.e., 350 BHMC steps, the same operators in the same order, the same seed for the random number generator, and so on. However, in this second run the AFO was enabled with η = 0.4. The global minimum structure identified in this run was the same as in the first, which are both the same as the one reported in the previous section for Al_{15}; however, the computational time

dx.doi.org/10.1021/ci400224z | J. Chem. Inf. Model. 2013, 53, 2282−2298

required was 53% lower than the first run. This comparison confirms the preceding discussion that the AFO is able to reduce computational time and still allow a fair exploration of the PES, yielding good results. Furthermore, there were no self-consistency problems in any of the DFT calculations carried out in the second run. In addition, the filter analysis described in this section for Al_{15} was performed for Al_{10}, Al_{20}, and Al_{25} as well, and the results were similar to those presented here.

IV. DISCUSSION AND SUMMARY

In this work, we summarized our suggestions and strategies to improve the BHMC algorithm in the search of the global minima of clusters and NPs described by empirical and first-principles (DFT-PBE) interacting potentials. The success of our BHMC implementation is based on three ideas.

(i) Exploration of the PES using a large set of trial operators, which are separated into two distinct groups, namely, local (CDO and GCDO) and nonlocal (TO, AO, SAO, IO, EO, GEO, OJ, Crossover) operators. Local operators provide the possibility for a local exploration of the PES using atomic displacements of one to N atoms near their atomic positions, while the nonlocal operators are designed to take the exploration from one region of the PES to another one, and hence, it helps to quickly overcome large potential energy barriers. Therefore, it is straightforward to realize that the application of local and nonlocal operators should be interposed along the BHMC optimization to achieve good efficiency, that is, once a good region in the PES is identified by a nonlocal operator, a local operator should have the chance to explore the region and lower the total energy of the system even further.

(ii) To improve the exploration of the PES as well as to deal with the acceptance rate problem within a large set of trial operators we proposed a static and a dynamic approach for the application of the trial operators. In the static approach, every trial operator is applied for a consecutive number of steps (input parameter), which can be different for each operator, while in the dynamic approach, a particular trial operator is employed to generate new configurations until it reaches a maximum number of consecutive rejections by the Metropolis criterion. Thus, a particular trial operator can contribute significantly to obtain the putative global minima for a particular system, while for a similar system that differs in a few atoms or the same system with a different initialization, the same operator might not have the same efficiency as the exploration of the PES can follow a path in which other trial operators can provide more significant contributions. The dynamic selection of the trial operators provides greater flexibility and allows an increased efficiency for every operator along of the optimization.

(iii) In particular, the use of nonlocal trial operators or local trial operators with the displacement of N atoms can lead to unphysical configurations, i.e., disconnected or overlapping atoms. To deal with this problem, which affects mainly BHMC-DFT calculations due to the problems in the self-consistent of the electron density, we designed a filter operator to avoid unphysical situations that are unlikely to occur in global minimum structures. We found that the filter operator contributes to improve the quality of the exploration of the configuration space and reduces computational time, and hence, it is fundamental to improve the chances of success in BHMC-DFT calculations.

These suggestions were the base of our BHMC implementation, which was applied for a large number of systems. We found the putative global minima for the well-known problem of the LJ_N (N = 2−147) and SC_N (N = 3−148) clusters and with a competitive rate of success (and in some cases higher) for most difficult cases. The study of the SC_N clusters was extended to the size range N = 81−148, which was previously available only for N = 3−80. We demonstrated that our implementation can handle large LJ_N NPs (N = 200, ..., 1500), using randomly initialized configurations without any bias. We also applied our implementation to BLJ clusters with fixed composition as a test case and to the $(AgPd)_{55}$ system described by the SC potential. The results for binary systems clearly show that our methodology is able to deal with complex cases without a significant increase of computational cost in comparison with single species systems of same size.

Beyond all those calculations for empirical potentials, our BHMC implementation employed first-principles DFT to describe the atomic structure of Al_N clusters (N = 2−30). Using BHMC-DFT for unbiased global optimization starting from randomly initialized structures we reproduced the majority of known results in the literature,[91] and a previously unknown global minimum structure was identified for Al_{24}, which confirms that our strategies increase the reliability of the BHMC algorithm as a stand-alone technique for first-principles global optimization.

By applying our BHMC implementation to a large number of structures corresponding to very different classes of systems we were able to match the greater part of the best results available in the literature. In many cases our strategies lead to improved efficiency, and moreover two previously unknown putative global minima were identified, BLJ_{38} and Al_{24}, even though these systems have been the target of numerous studies for the last years. We conclude that the strategies and ideas embedded in our implementation provide a significant contribution to the field of global optimization of atomic clusters and NPs.

APPENDIX: ADAPTIVE STEEPEST DESCENT ALGORITHM FOR LOCAL OPTIMIZATION

For LJ and SC systems up to 147 and 148 atoms, respectively, the procedure that we used to map the PES onto basins of attraction is an adaptive steepest descent algorithm, Figure 8, based on ref 122. This algorithm takes a set of atomic coordinates for N atoms ($\{\mathbf{R}\} = \mathbf{r}_1, \mathbf{r}_2,...,\mathbf{r}_N$), the set of forces acting upon each atom ($\{\mathbf{F}\} = \mathbf{F}_1,\mathbf{F}_2,...,\mathbf{F}_N$), a maximum number

1. $s \Leftarrow 1, \alpha \Leftarrow 0.05$
2. $E^s \Leftarrow E(\{\mathbf{R}^s\})$
3. Displace atoms $i = 1, \ldots, N$
   (a) Update $\mathbf{F}_i$
   (b) $\mathbf{r}_i^{s+1} \Leftarrow \mathbf{r}_i^s + \alpha \frac{\mathbf{F}_i}{|\mathbf{F}_i|}$
4. $E^{s+1} \Leftarrow E(\{\mathbf{R}^{s+1}\})$
5. If $E^{s+1} < E^s$ then increase α by 5%
6. Else decrease α by 40% and $\mathbf{R}^{s+1} \Leftarrow \mathbf{R}^s$
7. $s \Leftarrow s + 1$
8. If $\max(F_{i,j}) \leq \epsilon$ $(j = x, y, z)$ or $s > s_{\max}$ then stop
9. Else go to step 2.

Figure 8. Adaptive steepest descent algorithm.

dx.doi.org/10.1021/ci400224z | J. Chem. Inf. Model. 2013, 53, 2282−2298

of iterations (s_{max}), and a maximum tolerance for the final force components (ϵ). It proceeds then by displacing the coordinate $\mathbf{r}_i$ of each atom i toward the steepest decreasing direction on the PES, which is given by the direction of the force $\mathbf{F}_i$.

As shown in step 3-b of Figure 8, we obtain a unit vector in the direction of the force $\mathbf{F}_i$ and the length of the displacement in this direction is given by the parameter α. This algorithm is adaptive in the sense that α is adjusted automatically depending on whether the energy is lowered or not in a particular step, however without using a linear minimization procedure, which usually imposes a burden on computational cost. By using only the directions of the forces to perform a displacement, and not their magnitudes, the algorithm avoids too large displacements when two atoms are very close to each other, exerting a large force one upon another. In the BHMC runs for LJ and SC systems we used ϵ = 0.001 units of force and s_{max} = 1000, yielding energies that agree with reference data up to 6 and 4 decimal places for LJ and SC systems, respectively.

■ ASSOCIATED CONTENT

Supporting Information

Standard XYZ files with atomic positions and corresponding energies for the putative global minimum structures discussed in this work. This material is available free of charge via the Internet at http://pubs.acs.org.

■ AUTHOR INFORMATION

Corresponding Authors

*E-mail: rondina@usp.br.

*E-mail: juarez_dasilva@iqsc.usp.br.

Notes

The authors declare no competing financial interest.

■ ACKNOWLEDGMENTS

We thank the financial support of the São Paulo Science Foundation (FAPESP) and the Brazilian federal agency CAPES. We gratefully acknowledge the computing time provided in the Blue Gene/P supercomputer maintained by the Research Computing Support Group (Rice University) and the Laboratório de Computação Científica Avançada (Universidade de São Paulo). The infrastructure provided to our computer cluster by the Centro de Informática de São Carlos (Universidade de São Paulo) is acknowledged as well.

■ REFERENCES

(1) Castleman, A. W., Jr.; Jena, P. Clusters: A bridge across the disciplines of environment, material science, and biology. *Proc. Natl. Acad. Sci. U.S.A.* **2006**, *103*, 10554−10559.

(2) Piotrowski, M. J.; Piquini, P.; Da Silva, J. L. F. Density functional theory investigation of 3*d*, 4*d*, and 5*d* 13-atom metal clusters. *Phys. Rev. B* **2010**, *81*, 155446.

(3) Kelly, K. L.; Coronado, E.; Zhao, L. L.; Schatz, G. C. The optical properties of metal nanoparticles: The influence of size, shape, and dielectric environment. *J. Phys. Chem. B* **2003**, *107*, 668−677.

(4) Bansmann, J.; Baker, S. H.; Binns, C.; Blackman, J. A.; Bucher, J.-P.; Dorantes-Dávila, J.; Dupuis, V.; Favre, L.; Kechrakos, D.; Kleibert, A.; Meiwes-Broer, K.-H.; Pastore, G. M.; Perez, A.; Toulemonde, O.; Trohidou, K. N.; Tuaillon, J.; Xie, Y. Magnetic and structural properties of isolated and assembled clusters. *Surf. Sci. Rep.* **2005**, *56*, 189−275.

(5) Li, J.; Li, X.; Zhai, H.-J.; Wang, L.-S. Au_{20}: A tetrahedral cluster. *Science* **2003**, *299*, 864−867.

(6) Lopez, N.; Janssens, T. V. W.; Clausen, B. S.; Xu, Y.; Mavrikakis, M.; Bligaardd, T.; Nørskov, J. K. On the origin of the catalytic activity of gold nanoparticles for low-temperature CO oxidation. *J. Catal.* **2004**, *223*, 232−235.

(7) Pan, X.; Fan, Z.; Chen, W.; Ding, Y.; Luo, H.; Bao, X. Enhanced ethanol production inside carbon-nanotube reactors containing catalytic particles. *Nat. Mater.* **2007**, *6*, 507.

(8) El-Sayed, I. H.; Huang, X.; El-Sayed, M. A. Surface plasmon resonance scattering and absorption of anti-EGFR antibody conjugated gold nanoparticles in cancer diagnostics: Applications in oral cancer. *Nano Lett.* **2005**, *5*, 829−834.

(9) Narayanan, R.; El-Sayed, M. A. Shape-dependent catalytic activity of platinum nanoparticles in colloidal solution. *Nano Lett.* **2004**, *4*, 1343−1348.

(10) Scholl, J. A.; Koh, A. L.; Dionne, J. A. Quantum plasmon resonances of individual metallic nanoparticles. *Nature* **2012**, *483*, 421−427.

(11) Hoare, M. R. Structure and dynamics of simple microclusters. *Adv. Chem. Phys.* **1979**, *40*, 49−135.

(12) Tsai, C. J.; Jordan, K. D. Use of an eigenmode method to locate the stationary points on the potential energy surfaces of selected argon and water clusters. *J. Phys. Chem.* **1993**, *97*, 11227−11237.

(13) Doye, J. P. K.; Wales, D. J. Saddle points and dynamics of Lennard-Jones clusters, solids, and supercooled liquids. *J. Chem. Phys.* **2002**, *116*, 3777.

(14) Wales, D. J.; Doye, J. P. K. Stationary points and dynamics in high-dimensional systems. *J. Chem. Phys.* **2003**, *119*, 12409.

(15) Wales, D. J.; Bogdan, T. V. Potential energy and free energy landscapes. *J. Phys. Chem.* **2006**, *110*, 20765−20776.

(16) Hartke, B. Global geometry optimization of clusters using genetic algorithms. *J. Phys. Chem.* **1993**, *97*, 9973−9976.

(17) Daven, D.; Tit, N.; Morris, J.; Ho, K. Structural optimization of Lennard-Jones clusters by a genetic algorithm. *Chem. Phys. Lett.* **1996**, *256*, 195−200.

(18) Niesse, J. A.; Mayne, H. R. Global geometry optimization of atomic clusters using a modified genetic algorithm in space-fixed coordinates. *J. Chem. Phys.* **1996**, *105*, 4700.

(19) Johnston, R. L. Evolving better nanoparticles: Genetic algorithms for optimizing cluster geometries. *Dalton Trans.* **2003**, 4193−4207.

(20) Wales, D. J.; Doye, J. P. K. Global optimization by basin-hopping and the lowest energy structures of Lennard-Jones clusters containing up to 110 atoms. *J. Phys. Chem. A* **1997**, *101*, 5111−5116.

(21) Gehrke, R.; Reuter, K. Assessing the efficiency of first-principles basin-hopping sampling. *Phys. Rev. B* **2009**, *79*, 085412.

(22) Lee, J.; Lee, I.-H.; Lee, J. Unbiased global optimization of Lennard-Jones clusters for $N \leq 201$ using the conformational space annealing method. *Phys. Rev. Lett.* **2003**, *91*, 080201.

(23) Shao, X.; Cheng, L.; Cai, W. A dynamic lattice searching method for fast optimization of Lennard-Jones clusters. *J. Comput. Chem.* **2004**, *25*, 1693−1698.

(24) Pullan, W. An unbiased population-based search for the geometry optimization of Lennard-Jones clusters: $2 \leq N \leq 372$. *J. Comput. Chem.* **2005**, *26*, 899−906.

(25) Raphael, B.; Smith, I. F. C. A direct stochastic algorithm for global search. *Appl. Math. Comput.* **2003**, *146*, 729−758.

(26) Locatelli, M.; Schoen, F. Fast global optimization of difficult Lennard-Jones clusters. *Comput. Optim. Appl.* **2002**, *21*, 55−70.

(27) Wales, D. J.; Scheraga, H. A. Global optimization of clusters, crystals, and biomolecules. *Science* **1999**, *285*, 1368−1372.

(28) Baletto, F.; Ferrando, R. Structural properties of nanoclusters: Energetic, thermodynamic, and kinetic effects. *Rev. Mod. Phys.* **2005**, *77*, 371−423.

(29) Calvo, F. Non-genetic global optimization methods in molecular science: An overview. *Comput. Mater. Sci.* **2009**, *45*, 8−15.

(30) Catlow, C. R. A.; Bromley, S. T.; Hamad, S.; Mora-Fonz, M.; Sokol, A. A.; Woodley, S. M. Modelling nano-clusters and nucleation. *Phys. Chem. Chem. Phys.* **2010**, *12*, 786−211.

(31) Hartke, B. Global optimization. *Wiley Interdiscip. Rev.: Comput. Mol. Sci.* **2011**, *1*, 879−887.

(32) Li, Z.; Scheraga, H. A. Monte Carlo-minimization approach to the multiple-minima problem in protein folding. *Proc. Natl. Acad. Sci. U.S.A.* **1987**, *84*, 6611−6615.
(33) Doye, J. P. K.; Wales, D. J. Global minima for transition metal clusters described by Sutton-Chen potentials. *New. J. Chem.* **1998**, *22*, 733−744.
(34) Leary, R. H. Global optimization on funneling landscapes. *J. Global Optim.* **2000**, *18*, 367−383.
(35) Locatelli, M.; Schoen, F. Efficient algorithms for large scale global optimization: Lennard-Jones clusters. *Comput. Optim. Appl.* **2003**, *26*, 173−190.
(36) Goedecker, S. Minima hopping: An efficient search method for the global minimum of the potential energy surface of complex molecular systems. *J. Chem. Phys.* **2004**, *120*, 9911.
(37) Iwamatsu, M.; Okabe, Y. Basin hopping with occasional jumping. *Chem. Phys. Lett.* **2004**, *389*, 396−400.
(38) Zhan, L.; Piwowar, B.; Liu, W.-K.; Hsu, P. J.; Lai, S. K.; Chen, J. Z. Y. Multicanonical basin hopping: A new global optimization method for complex systems. *J. Chem. Phys.* **2004**, *120*, 5536.
(39) Zhan, L.; Chen, J. Z. Y.; Liu, W.-K. Monte Carlo basin paving: An improved global optimization method. *Phys. Rev. E* **2006**, *73*, 015701.
(40) Zhan, L.; Chen, J. Z. Y.; Liu, W. K.; Lai, S. K. Asynchronous multicanonical basin hopping method and its application to cobalt nanoclusters. *J. Chem. Phys.* **2005**, *122*, 244707.
(41) Bandyopadhyay, P. Two-surface Monte Carlo with basin hopping: Quantum mechanical trajectory and multiple stationary points of water cluster. *J. Chem. Phys.* **2008**, *128*, 134103.
(42) Cheng, L.; Feng, Y.; Yang, J.; Yang, J. Funnel hopping: Searching the cluster potential energy surface over the funnels. *J. Chem. Phys.* **2009**, *130*, 214112.
(43) Grosso, A.; Locatelli, M.; Schoen, F. Solving molecular distance geometry problems by global optimization algorithms. *Comput. Optim. Appl.* **2009**, *43*, 23−37.
(44) Lai, X.; Xu, R.; Huang, W. Geometry optimization of bimetallic clusters using an efficient heuristic method. *J. Chem. Phys.* **2011**, *135*, 164109.
(45) Wales, D. J.; Head-Gordon, T. Evolution of the potential energy landscape with static pulling force for two model proteins. *J. Phys. Chem. B* **2012**, *116*, 8394−8411.
(46) Wales, D. J. GMIN: A program for finding global minima and calculating thermodynamic properties from basin-sampling. http://www-wales.ch.cam.ac.uk/software.html (accessed August 18, 2013).
(47) Strodel, B.; Lee, J. W. L.; Whittleston, C. S.; Wales, D. J. Transmembrane structures for Alzheimer's Aβ1−42 Oligomers. *J. Am. Chem. Soc.* **2010**, *132*, 13300−13312.
(48) Oakley, M. T.; Johnston, R. L.; Wales, D. J. Symmetrisation schemes for global optimization of atomic clusters. *Phys. Chem. Chem. Phys.* **2013**, *15*, 3965−3976.
(49) Kiran, B.; Bulusu, S.; Zhai, H.-J.; Yoo, S.; Zeng, X. C.; Wang, L.-S. Planar-to-tubular structural transition in boron clusters: B_{20} as the embryo of single-walled boron nanotubes. *Proc. Natl. Acad. Sci. U.S.A.* **2005**, *102*, 961−964.
(50) Yoo, S.; Zeng, X. C. Motif transition in growth patterns of small to medium-sized silicon clusters. *Angew. Chem., Int. Ed.* **2005**, *44*, 1491−1494.
(51) Aprá, E.; Ferrando, R.; Fortunelli, A. Density-functional global optimization of gold nanoclusters. *Phys. Rev. B* **2006**, *73*, 205414.
(52) Bulusu, S.; Zeng, X. C. Structures and relative stability of neutral gold clusters: Au_n (n = 15−19). *J. Chem. Phys.* **2006**, *125*, 154303.
(53) Shao, N.; Huang, W.; Gao, Y.; Wang, L.-M.; Li, X.; Wang, L.-S.; Zeng, X. C. Probing the structural evolution of medium-sized gold clusters: Au_n^- (n = 27 - 35). *J. Am. Chem. Soc.* **2010**, *132*, 6596−6605.
(54) Yoo, S.; Zeng, X. C. Global geometry optimization of silicon clusters described by three empirical potentials. *J. Chem. Phys.* **2003**, *119*, 1442−1450.
(55) Flikkema, E.; Bromley, S. T. Dedicated global optimization search for ground state silica nanoclusters: $(SiO_2)_N$ (N = 6−12). *J. Phys. Chem. B* **2004**, *108*, 9638−9645.
(56) Hamad, S.; Catlow, C. R. A.; Woodley, S. M.; Lago, S.; Mejías, J. A. Structure and stability of small TiO_2 nanoparticles. *J. Phys. Chem. B* **2005**, *109*, 15741−15748.
(57) Harding, D.; Mackenzie, S. R.; Walsh, T. R. Structural isomers and reactivity for Rh_6 and Rh_6^+. *J. Phys. Chem. B* **2006**, *110*, 18272−18277.
(58) Walsh, T. R. Relaxation dynamics and structural isomerism in Nb_{10} and Nb_{10}^+. *J. Chem. Phys.* **2006**, *124*, 204317.
(59) Da Silva, J. L. F.; Kim, H. G.; Piotrowski, M. J.; Prieto, M. J.; Tremiliosi-Filho, G. Reconstruction of core and surface nanoparticles: The example of Pt_{55} and Au_{55}. *Phys. Rev. B* **2010**, *82*, 205424.
(60) Aguado, A.; López, J. M. Structure determination in 55−atom Li-Na and Na-K nanoalloys. *J. Chem. Phys.* **2010**, *133*, 094302.
(61) Aguado, A.; Kostko, O. First-principles determination of the structure of Na_N and Na_N^- clusters with up to 80 atoms. *J. Chem. Phys.* **2011**, *134*, 164304.
(62) Garzón, I. L.; Michaelian, K.; Beltrán, M. R.; Posada-Amarillas, A.; Ordejón, P.; Artacho, E.; Sánchez-Portal, D.; Soler, J. M. Lowest energy structures of gold nanoclusters. *Phys. Rev. Lett.* **1998**, *81*, 1600−1603.
(63) Rossi, G.; Rapallo, A.; Mottet, C.; Fortunelli, A.; Baletto, F.; Ferrando, R. Magic polyicosahedral core-shell clusters. *Phys. Rev. Lett.* **2004**, *93*, 105503.
(64) Sutton, A. P.; Chen, J. Long-range Finnis-Sinclair potentials. *Philos. Mag. Lett.* **1990**, *61*, 139−146.
(65) Çağin, T.; Qi, Y.; Li, H.; Kimura, Y.; Ikeda, H.; Johnson, W. L.; Goddard, W. A., III. Calculation of mechanical, thermodynamic and transport properties of metallic glass formers. *MRS Symp. Ser.* **1999**, *554*, 43−48.
(66) Press, W. H.; Teukolsky, S. A.; Vetterling, W. T.; Flannery, B. P. *Numerical Recipes 3rd ed.: The Art of Scientific Computing*, 3rd ed.; Cambridge University Press: 2007.
(67) White, R. P.; Mayne, H. R. An investigation of two approaches to basin hopping minimization for atomic and molecular clusters. *Chem. Phys. Lett.* **1998**, *289*, 463−468.
(68) Kim, H. G.; Choi, S. K.; Lee, H. M. New algorithm in the basin hopping Monte Carlo to find the global minimum structure of unary and binary metallic nanoclusters. *J. Chem. Phys.* **2008**, *128*, 144702.
(69) Cai, W.; Feng, Y.; Shao, X.; Pan, Z. Optimization of Lennard-Jones atomic clusters. *J. Mol. Struct.* **2002**, *579*, 229−234.
(70) Cordero, B.; Gómez, V.; Platero-Prats, A. E.; Revés, M.; Echeverría, J.; Cremades, E.; Barragán, F.; Alvarez, S. Covalent radii revisited. *Dalton Trans.* **2008**, 2832−2838.
(71) Dai, Y.-H.; Liao, L.-Z. New conjugacy conditions and related nonlinear conjugate gradient methods. *Appl. Math. Optim.* **2001**, *43*, 87−101.
(72) Nocedal, J.; Wright, S. *Numerical Optimization*; Spinger: 2006.
(73) Blum, V.; Gehrke, R.; Hanke, F.; Havu, P.; Havu, V.; Ren, X.; Reuter, K.; Scheffler, M. Ab initio molecular simulations with numeric atom-centered orbitals. *Comput. Phys. Commun.* **2009**, *180*, 2175−2196.
(74) Frenkel, D.; Smit, B. *Understanding Molecular Simulation*; Academic Press Inc.: San Diego, 2002.
(75) Rossi, G.; Ferrando, R. Searching for low-energy structures of nanoparticles: a comparison of different methods and algorithms. *J. Phys.: Condens. Matter* **2009**, *21*, 084208.
(76) Lai, S. K.; Hsu, P. J.; Wu, K. L.; Liu, W. K.; Iwamatsu, M. Structures of metallic clusters: Mono- and polyvalent metals. *J. Chem. Phys.* **2002**, *117*, 10715.
(77) Ye, T.; Xu, R.; Huang, W. Global optimization of binary Lennard-Jones clusters using three perturbation operators. *J. Chem. Inf. Model.* **2011**, *51*, 572−577.
(78) Takeuchi, H. Novel method for geometry optimization of molecular clusters: Application to benzene cluster. *J. Chem. Inf. Model.* **2007**, *47*, 104−109.
(79) Bochicchio, D.; Ferrando, R. Size-dependent transition to high-symmetry chiral structures in AgCu, AgCo, AgNi, and AuNi nanoalloys. *Nano Lett.* **2010**, *10*, 4211−4216.

(80) Roberts, C.; Johnston, R. L.; Wilson, N. T. A genetic algorithm for the structural optimization of Morse clusters. *Theor. Chem. Acc.* **2000**, *104*, 123−130.
(81) Goldberg, D. E. *Genetic Algorithms in Search, Optimization, and Machine Learning*; Addison-Wesley Professional: 1989.
(82) Bochicchio, D.; Ferrando, R. Structure and thermal stability of AgCu chiral nanoparticles. *Eur. Phys. J. D* **2012**, *66*, 115.
(83) Gelman, A.; Gilks, W. R.; Roberts, G. O. Weak convergence and optimal scaling of random walk Metropolis algorithms. *Ann. Appl. Probab.* **1997**, *7*, 110−120.
(84) Kittel, C. *Introduction to Solid State Physics*; John Wiley & Sons, Inc.: Hoboken, NJ, 2005.
(85) Honeycutt, J. D.; Andersen, H. C. Molecular-dynamics study of melting and freezing of small, Lennard-Jones clusters. *J. Phys. Chem.* **1987**, *91*, 4950−4963.
(86) Northby, J. A. Structure and binding of Lennard-Jones clusters: $13 \leq N \leq 147$. *J. Chem. Phys.* **1987**, *87*, 6166−6177.
(87) Hohenberg, P.; Kohn, W. Inhomogeneous electron gas. *Phys. Rev.* **1964**, *136*, B864.
(88) Kohn, W.; Sham, L. J. Self-consistent equations including exchange and correlation effects. *Phys. Rev.* **1965**, *140*, A1133.
(89) Perdew, J. P.; Burke, K.; Ernzerhof, M. Generalized gradient approximation made simple. *Phys. Rev. Lett.* **1996**, *77*, 3865.
(90) Gehrke, R.; Gruene, P.; Fielicke, A.; Meijer, G.; Reuter, K. Nature of Ar bonding to small Co_n^+ clusters and its effect on the structure determination by far-infrared absorption spectroscopy. *J. Chem. Phys.* **2009**, *130*, 034306.
(91) Drebov, N.; Ahlrichs, R. Structures of Al_n, its anions and cations up to $n = 34$: A theoretical investigation. *J. Chem. Phys.* **2010**, *132*, 164703.
(92) Wales, D. J. OPTIM: A program for optimizing geometries and calculating reaction pathways. http://www-wales.ch.cam.ac.uk/software.html (accessed August 18, 2013).
(93) Wales, D. J.; Doye, J. P. K.; Dullweber, A.; Hodges, M. P.; Naumkin, F. Y.; Calvo, F.; Hernández-Rojas, J.; Middleton, T. F. The Cambridge Cluster Database (CCD). http://www-wales.ch.cam.ac.uk/CCD.html (accessed August 18, 2013).
(94) Hoare, M. R.; Pal, P. Physical cluster mechanics: Statics and energy surfaces for monatomic systems. *Adv. Phys.* **1971**, *20*, 161−196.
(95) Hoare, M. R.; Pal, P. Statics and stability of small cluster nuclei. *Nature Phys. Sci.* **1971**, *230*, 5−8.
(96) Gómez, S.; Romero, D. *Proceedings of the First European Congress of Mathematics*; Birkhäuser: Basel, 1994; Vol. *III*, pp 503−509.
(97) Pillardy, J.; Piela, L. Molecular dynamics on deformed potential energy hypersurfaces. *J. Chem. Phys.* **1995**, *99*, 11805−11812.
(98) Doye, J. P. K.; Wales, D. J.; Berry, R. S. The effect of the range of the potential on the structures of clusters. *J. Chem. Phys.* **1995**, *103*, 4234−4249.
(99) Doye, J. P.; Wales, D. J. Magic numbers and growth sequences of small face-centered-cubic and decahedral clusters. *Chem. Phys. Lett.* **1995**, *247*, 339−347.
(100) Leary, R. H.; Doye, J. P. K. Tetrahedral global minimum for the 98−atom Lennard-Jones cluster. *Phys. Rev. E* **1999**, *60*, R6320−R6322.
(101) Marks, L. D. Experimental studies of small particle structures. *Rep. Prog. Phys.* **1994**, *57*, 603−649.
(102) Xiang, Y.; Jiang, H.; Cai, W.; Shao, X. An efficient method based on lattice construction and the genetic algorithm for optimization of large Lennard-Jones clusters. *J. Phys. Chem. A* **2004**, *108*, 3586−3592.
(103) Xiang, Y.; Cheng, L.; Cai, W.; Shao, X. Structural distribution of Lennard-Jones clusters containing 562 to 1000 atoms. *J. Phys. Chem. A* **2004**, *108*, 9516−9520.
(104) Shao, X.; Xiang, Y.; Cai, W. Structural transition from icosahedra to decahedra of large Lennard-Jones clusters. *J. Phys. Chem. A* **2005**, *109*, 5193−5197.
(105) Yang, X.; Cai, W.; Shao, X. A dynamic lattice searching method with constructed core for optimization of large Lennard-Jones clusters. *J. Comput. Chem.* **2007**, *28*, 1427−1433.
(106) Xue, G. Molecular conformation on the CM-5 by parallel two-level simulated annealing. *J. Global Optim.* **1994**, *4*, 187−208.
(107) Romero, D.; Barrón, C.; Gómez, S. The optimal geometry of Lennard-Jones clusters: 148−309. *Comput. Phys. Commun.* **1999**, *123*, 87−96.
(108) Krivov, S. V. Hierarchical global optimization of quasiseparable systems: Application to Lennard-Jones clusters. *Phys. Rev. E* **2002**, *66*, 025701.
(109) Goedecker, S. In *Modern Methods of Crystal Structure Prediction*; Oganov, A. R., Ed.; Wiley-VCH Verlag GmbH & Co. KGaA: Weinheim, Germany, 2011; Chapter 6, pp 131−145.
(110) Grigoryan, V. G.; Alamanova, D.; Springborg, M. Structure and energetics of Cu_N clusters with $2 \leq N \leq 150$: An embedded-atom-method study. *Phys. Rev. B* **2006**, *73*, 115415.
(111) Wayne Pullan found three structures according to the Cambridge Cluster Database.
(112) Doye, J. P. K.; Meyer, L. Mapping the magic numbers in binary Lennard-Jones clusters. *Phys. Rev. Lett.* **2005**, *95*, 063401.
(113) Cassioli, A.; Locatelli, M.; Schoen, F. Global optimization of binary Lennard-Jones clusters. *Optim. Method Softw.* **2009**, *24*, 819−835.
(114) Kolossváry, I.; Bowers, K. J. Global optimization of additive potential energy functions: Predicting binary Lennard-Jones clusters. *Phys. Rev. E* **2010**, *82*, 056711.
(115) Sicher, M.; Mohr, S.; Goedecker, S. Efficient moves for global geometry optimization methods and their application to binary systems. *J. Chem. Phys.* **2011**, *134*, 044106.
(116) Hoppe, R. The coordination number − an "Inorganic chameleon". *Angew. Chem. Int. Ed.* **1970**, *9*, 25−34.
(117) Aguado, A.; López, J. M. Structures and stabilities of Al_n^+, Al_n, and Al_n^- ($n = 13 - 24$) clusters. *J. Chem. Phys.* **2009**, *130*, 064704.
(118) Momma, K.; Izumi, F. VESTA 3 for three-dimensional visualization of crystal, volumetric and morphology data. *J. Appl. Crystallogr.* **2011**, *44*, 1272−1276.
(119) Kaxiras, E. *Atomic and Electronic Structure of Solids*; Cambridge University Press: Cambridge, 2003.
(120) Cox, D. M.; Trevor, D. J.; Whetten, R. L.; Rohlfing, E. A.; Kaldor, A. Aluminum clusters: Magnetic properties. *J. Chem. Phys.* **1986**, *84*, 4651−4656.
(121) Li, X.; Wu, H.; Wang, X.-B.; Wang, L.-S. s-p hybridization and electron shell structures in aluminum clusters: A photoelectron spectroscopy study. *Phys. Rev. Lett.* **1998**, *81*, 1909−1912.
(122) Shewchuk, J. R. *An introduction to the conjugate gradient methods without the agonizing pain*; Tech. Rep. CMU-CS-94-125; 1994.